SANDIA REPORT

SAND2005-7791
Unlimited Release
Printed January 2006

Systematic Evaluation of Satellite Remote Sensing for Identifying Uranium Mines and Mills

Christopher L. Stork, Heidi A. Smartt, Dianna S. Blair, and Jody L. Smith

Prepared by
Sandia National Laboratories
Albuquerque, New Mexico 87185 and Livermore, California 94550

Sandia is a multiprogram laboratory operated by Sandia Corporation,
a Lockheed Martin Company, for the United States Department of Energy's
National Nuclear Security Administration under Contract DE-AC04-94AL85000.

Issued by Sandia National Laboratories, operated for the United States Department of Energy by Sandia Corporation.

Available to DOE and DOE contractors from
U.S. Department of Energy
Office of Scientific and Technical Information
P.O. Box 62
Oak Ridge, TN 37831

Telephone: (865)576-8401
Facsimile: (865)576-5728
E-Mail: reports@adonis.osti.gov
Online ordering: http://www.osti.gov/bridge

Available to the public from
U.S. Department of Commerce
National Technical Information Service
5285 Port Royal Rd
Springfield, VA 22161

Telephone: (800)553-6847
Facsimile: (703)605-6900
E-Mail: orders@ntis.fedworld.gov
Online order: http://www.ntis.gov/help/ordermethods.asp?loc=7-4-0#online

SAND2005-7791
Unlimited Release
Printed February 2006

Systematic Evaluation of Satellite Remote Sensing for Identifying Uranium Mines and Mills

Christopher L. Stork, Heidi A. Smartt, Dianna S. Blair, and Jody L. Smith
Sandia National Laboratories
P.O. Box 5800
Albuquerque, New Mexico 87185-0886

Abstract

In this report, we systematically evaluate the ability of current-generation, satellite-based spectroscopic sensors to distinguish uranium mines and mills from other mineral mining and milling operations. We perform this systematic evaluation by (1) outlining the remote, spectroscopic signal generation process, (2) documenting the capabilities of current commercial satellite systems, (3) systematically comparing the uranium mining and milling process to other mineral mining and milling operations, and (4) identifying the most promising observables associated with uranium mining and milling that can be identified using satellite remote sensing. The Ranger uranium mine and mill in Australia serves as a case study where we apply and test the techniques developed in this systematic analysis. Based on literature research of mineral mining and milling practices, we develop a decision tree which utilizes the information contained in one or more observables to determine whether uranium is possibly being mined and/or milled at a given site. Promising observables associated with uranium mining and milling at the Ranger site included in the decision tree are uranium ore, sulfur, the uranium pregnant leach liquor, ammonia, and uranyl compounds and sulfate ion disposed of in the tailings pond. Based on the size, concentration, and spectral characteristics of these promising observables, we then determine whether these observables can be identified using current commercial satellite systems, namely Hyperion, ASTER, and Quickbird. We conclude that the only promising observables at Ranger that can be uniquely identified using a current commercial satellite system (notably Hyperion) are magnesium chlorite in the open pit mine and the sulfur stockpile. Based on the identified magnesium chlorite and sulfur observables, the decision tree narrows the possible mineral candidates at Ranger to uranium, copper, zinc, manganese, vanadium, the rare earths, and phosphorus, all of which are milled using sulfuric acid leaching.

Acknowledgments

The authors thank Paul Mendoza at Los Alamos National Laboratory for useful discussions regarding the spectral properties of aqueous uranyl compounds. The authors also thank Jeffrey Mercier (Org. 5712) for his help in generating the pan-sharpened Quickbird images of the Ranger mine and mill.

Contents

Figures

Tables

Nomenclature

ASTER Advanced Spaceborne Thermal Emission and Reflection Radiometer
EO-1 Earth Observing-1
ETM Enhanced Thematic Mapper
GSD Ground Spatial Distance
IAEA International Atomic Energy Agency
IR Infrared
MSS Multi-Spectral Scanner
PLL Pregnant Leach Liquor
RGB Red-Green-Blue
SLC Scan Line Corrector
SNL Sandia National Laboratories
SWIR Short Wave Infrared
TIR Thermal Infrared
TM Thematic Mapper
VNIR Visible and near infrared
WFT Wide Field Telescope

This page intentionally left blank.

1. Introduction

Uranium deposits are found throughout the world with the largest deposits located in Australia (28%), Kazakhstan (18%), Canada (12%), South Africa (8%), and Namibia (6%) [1]. As these and other states sign up to the Additional Protocol to their Safeguards Agreements with the International Atomic Energy Agency (IAEA), they will need to declare a broader scope of their nuclear activities, including uranium mining and milling activities. This could significantly increase the burden on IAEA resources for safeguards implementation at uranium mines and mills in terms of inspector time and monitoring technology deployed.

There is considerable interest at the International Atomic Energy Agency (IAEA) and other nuclear regulatory agencies in utilizing satellite remote sensing for the identification of undeclared uranium mining and milling activities and the verification of declared uranium mining and milling operations [2]. The use of satellite remote sensing by the international nuclear regulatory community is seen as a way to reduce monitoring costs while improving inspection performance. Satellite remote sensing offers the ability to monitor activities over a large spatial region in a non-intrusive manner, and, therefore, the use of satellite imagery could potentially reduce or even eliminate the need for inspectors at uranium mining and milling sites.

Despite the potential advantages of using satellite remote sensing for monitoring uranium mining and milling, a systematic evaluation of the utility of satellite remote sensing in differentiating uranium mining and milling from other types of mineral mining and milling has not been performed. Previous studies on using remote sensing for monitoring uranium mining and milling have been anecdotal case studies as opposed to systematic analyses. These previous studies can be divided into two categories: those that seek unique features of a uranium mine and mill to identify potential clandestine activities, and those that seek verification of State Declarations, such as movement of material. In a conference paper, Troung *et al* [3] analyzed multispectral IKONOS imagery and hyperspectral Hyperion imagery to determine if they could confirm operations, scheduling, and movement of materials. The authors found that IKONOS was able to discriminate between different ore piles by grouping spectrally similar objects, while Hyperion detected possible high particle content in the tailings ponds. This information was used for change analysis. In a similar paper [4], the objective was to confirm that operations reported by the States to the IAEA were consistent. Panchromatic images were used to compare the layouts, locations, consistency of scales with declared production levels, and operational status to those provided by the States. This paper identified discriminator stations as a unique feature of uranium mines, but pointed out that the station could not be differentiated from a refueling station from the images. For the Ranger uranium mine and mill in Australia, the size and extent of the sulfur and coarse ore stockpiles as well as traffic through the discriminator station are key features used to estimate the rate of uranium production. The multispectral and hyperspectral images were used to look at the tailings in the ponds and determine if over a period of six months or

longer these had changed, providing an indication of the uranium production rate at the mine. Previous studies involving the detection of uranium mines can be found in a paper by Neville *et al* [5], where some extracted endmember spectra representative of a uranium mine in Northern Saskatchewan are presented, and in a paper by Levesque *et al* [6], which seeks to identify uranium mine tailings. In the Levesque paper [6], an airborne hyperspectral sensor, Probe-1, took images over the Pronto mine tailings near Elliot Lake, Ontario, Canada, in 1999. The goal was to determine if uranium mine tailings could be distinguished from other types of mine tailings using unique mineral absorption features. However, no such features were discovered.

In this report, we address this deficiency in the current knowledge base and systematically evaluate the ability of current-generation, satellite-based spectroscopic sensors to distinguish uranium mines and mills from other types of mineral mining and milling operations. We perform this systematic evaluation by (1) outlining the remote, spectroscopic signal generation process, (2) documenting the capabilities of current commercial satellite systems, (3) systematically comparing the uranium mining and milling process to other types of mineral mining and milling operations, and (4) identifying the most promising observables associated with uranium mining and milling that can be identified using satellite remote sensing. It is important to outline the remote, spectroscopic signal generation process in order to understand which portions of the electromagnetic spectrum can be used to remotely monitor mining and milling activity. Documenting the capabilities of current commercial satellite systems is important to understand spectral and spatial resolution limitations which may limit mining and milling monitoring. Performing a systematic comparison of uranium mining and milling to other types of mineral mining and milling operations is key in identifying observables unique to or characteristic of uranium mining and milling. Based on this comparison, we identify the most promising observables associated with uranium mining and milling that can be exploited remotely.

There are a large number of uranium mining and milling operations distributed throughout the world employing different processes to extract uranium from the ore. We use the Ranger uranium mine and mill in Australia [7], which is a well-known site that has a large body of open literature information, to illustrate the systematic approach we are proposing. The Ranger uranium mine and mill serves as a case study where we apply and evaluate the techniques developed in this systematic analysis.

2. Sensor Principles and Background

2.1. Spectroscopy to Imaging

Spectroscopy has been used in the laboratory by physicists and chemists for over 100 years to record information directly related to the chemical bonds in molecules. By measuring the specific wavelengths of radiation that are absorbed by a sample, a unique "fingerprint" of the material is obtained.

A spectrometer records the photons in the instrument field of view that strike the detector. The photons are collected at particular wavelengths using some form of dispersive element or filter mechanism. An imaging spectrometer expands this concept by using an array of detectors. The imaging spectrometer captures photons from each subregion in a larger area onto individual detectors, resulting in an image of the area. This approach, which provides material interaction information about different areas on a sample, has a number of data tradeoffs that will be discussed later. In a laboratory, sample conditions and the instrument environment can be tightly controlled. This is critical because light interacts with all matter, in absorption, reflection, and emission modes. The interacting media can be the sample of interest, the environment around the sample, or changes in the instrument itself. Advances in technology have improved the stability of instruments, allowing them to be used outside the laboratory. But the above issues remain.

Applications benefited from technology developments, and robust systems were identified to be flown on airborne platforms to study wide geographic areas. The first imaging systems to be deployed on airborne platforms utilized broad spectral bands in the visible range. These systems, known as panchromatic instruments, result in black and white images, i.e. photographs, of the sample area. Generally these images do not contain radiometric information. Analysis of these images is performed visually for shape and contrast content.

The second generation of instruments were known as multispectral with a few bands ranging from 0.4 to 1.1 μm (four bands) and a thermal band at 10.4-12.6 μm. The third generation satellites, Landsat-4 to Landsat-7, carried sensors with seven spectral bands ranging from 0.45 to 0.9 μm (four bands), 1.55-1.75 μm (band five), 2.08-2.35 μm (band six) and a thermal band with 10.4-12.5 μm wavelengths. The Landsat-7 sensor had an additional panchromatic band (0.50-0.90 μm). A fourth generation instrument was placed on board the ASTER satellite, acquiring information across 14 spectral bands. Multispectral instruments provide general classes of chemical information. The development of hyperspectral instruments followed multispectral systems. By definition, hyperspectral instruments acquire information across 100 or more spectral channels. Launched onboard the Earth Observing-1 (EO-1) spacecraft in November 2000, the Hyperion hyperspectral imager observes the earth in 220 spectral bands from the visible to the shortwave infrared (0.40 to 2.50 μm). Details on the spatial and spectral capabilities of the Hyperion, Landsat-5, Landsat-7, and ASTER instruments are provided in section 3 of this report.

2.2. Spectral Component to Imaging

As stated earlier, when moving from the controlled environment of a laboratory to the field, complex interactions of light with matter will manifest themselves in the data. The farther the sample is from the detector, the greater the impact of these complexities. This became obvious as imaging systems were placed on airborne and satellite platforms miles away from the material they were analyzing. In the laboratory, the photons incident upon a sample, and the collection geometry of the sample, is controlled by the experimentalist. The spatial extent of the material of interest is controlled to provide optimum sensor fill and geometry. This is not possible with the large sample area being investigated using platform-based imaging systems. Furthermore, in the laboratory, the source is fully characterized and can readily be subtracted from the data, leaving only the signature of the compound of interest. For the passive imaging systems of interest here, the source is the sun for daytime collections and self-emission of the target for nighttime imaging. To obtain the material features, this variable source must be removed from the data, leaving only the signature of the interaction.

The intervening atmosphere also provides significant interaction. Because of the complexity of all the interactions of the source prior to reaching the sensor, there is significant signal preprocessing that is necessary to extract a ground signature. This is done using one of various available models. To improve the accuracy of the results, these models require inputs that define current atmospheric conditions such as temperature, pressure, aerosol density and size distribution.

For remote imaging of solids in the visible to shortwave infrared, the primary property of interest is reflectance. Individual materials reflect the light in a very specific way as a function of wavelength that provides a unique signature for most materials. Typically satellite and airborne systems are calibrated to report radiance (Watts/m^2/μm/sr) that is incident on the detector.

In the visible to shortwave infrared, the radiation measured by a remote instrument originates from the sun. The total at-sensor, solar radiation can be modeled by the following equation [8]:

$$L_\lambda^s(x,y) = \rho(x,y,\lambda)\frac{\tau_v(\lambda)}{\pi}\left[\tau_s(\lambda)E_\lambda^0\cos\left[\theta(x,y)\right] + F(x,y)E_\lambda^d\right] + L_\lambda^{sp}$$

where x and y designate spatial coordinates, λ designates wavelength, ρ is the diffuse spectral reflectance of the surface, $\tau_v(\lambda)$ is the view path transmittance, E_λ^0 is the spectral irradiance, θ is the incident angle, $F(x,y)$ is a topographic factor, E_λ^d is the irradiance at the surface due to skylight, and L_λ^{sp} is the up-scattered path radiance. The intervening atmosphere has a profound effect on the at-sensor signal. Along the solar path between the sun and the earth, the atmosphere absorbs and scatters radiation, and again along the view path between the earth and the sensor. Figure 1 depicts a typical solar path transmittance in the visible and shortwave infrared region. The characteristics of the atmospheric transmittance determine which parts of the spectrum can be exploited

remotely. As an example, the strong molecular absorption bands of atmospheric water and carbon dioxide near 1.4 μm and 1.9 μm completely block transmission of radiation in these spectral regions.

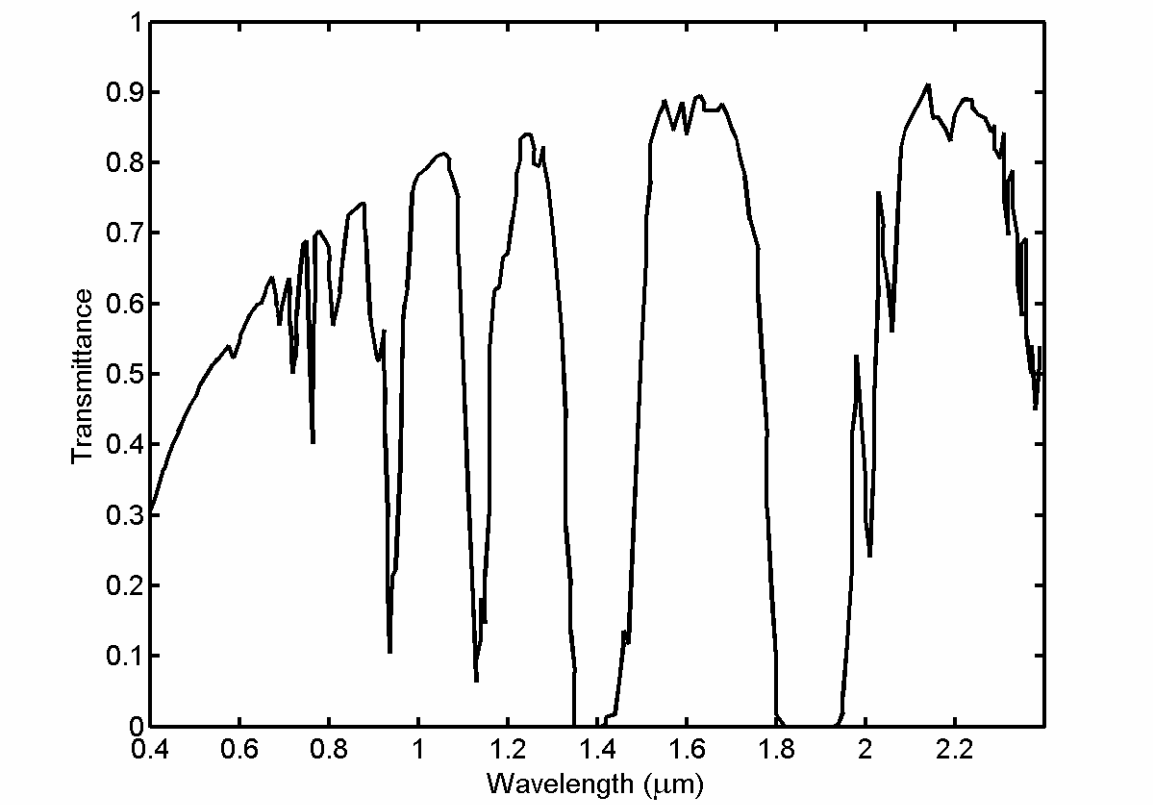

Figure 1. Typical solar path transmittance in the visible and shortwave infrared.

The radiance measurement at the sensor itself does not directly provide information about the material of interest. The data collected by multispectral and hyperspectral sensors generally are processed by the analyst into reflectance units, allowing for mathematical manipulation and direct comparison to pure material obtained in the laboratory. However, this processing of the image data to reveal ground reflectance is not trivial. A thorough understanding of solar radiation and its interaction with atmospheric constituents is needed, along with the exact geometry of the collection. Accurate detection and identification of materials is dependent on the spectral coverage, spectral resolution, signal-to-noise of the spectrometer, the abundance of the material and the strength of absorption features for that material in the wavelength region measured.

Figure 2 is an illustration of both multispectral data, typically identified as five to twenty moderately wide spectral bands, and hyperspectral data, identified as hundreds of narrow spectral bands with a bandwidth of approximately 10 nm. These plots demonstrate the

relative data differences of the two techniques. Intended to illustrate the distinct signature or spectral response, at about 0.68 μm, caused by chlorophyll and commonly referred to as the "red edge", this figure also shows the more detailed chemical information contained in hyperspectral data.

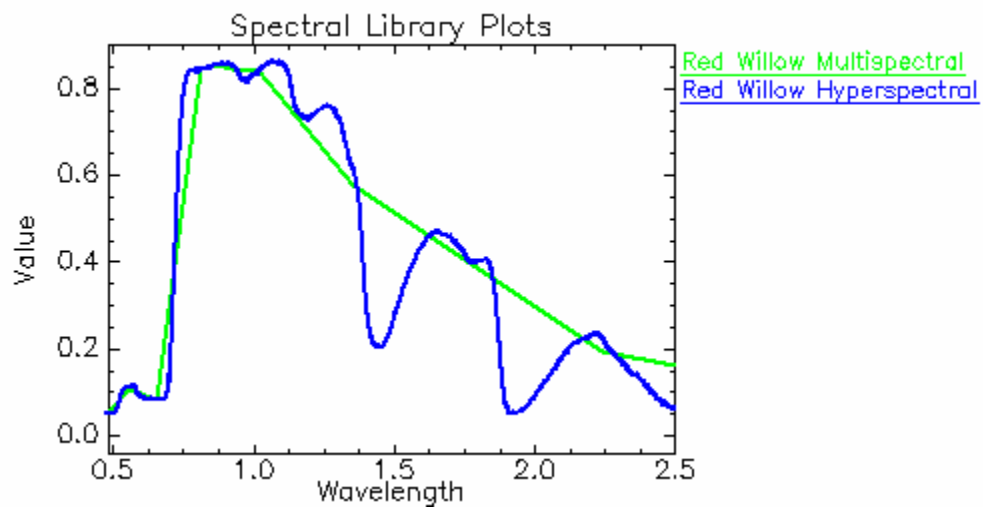

Figure 2. Hyperspectral and multispectral vegetation signatures illustrating the "red edge".

2.3. Spatial Aspect to Imaging

The ability to identify spectral signatures of specific materials is highly dependent upon both the spectral and spatial resolution of the data. There are a limited number of photons reflected from the earth's surface. To provide adequate photons at the sensor, the ground sample distance (GSD) or ground pixel size must be balanced with the number of spectral bands. As detectors have become more sensitive, hyperspectral instruments have become a reality. However they must integrate the signal over a larger spatial pixel to obtain sufficient signal in each of the narrow spectral bands. For the same reasons, single band panchromatic instruments have the best spatial resolution with multispectral instruments somewhere between these two extremes. Therefore, high spatial resolution imagery can significantly aid and complement the interpretation of high spectral resolution images, which necessarily suffer from poorer spatial discrimination.

Geology was one of the first disciplines to benefit from hyperspectral remote sensing. Therefore, most theory is developed relative to earth material interactions. Increasingly, vegetation-based research is utilizing tools and techniques developed from geology. This type of successful identification from hyperspectral sensors is highly dependent upon the GSD and the spatial extent of the materials of interest (e.g. how much area is covered predominantly by the material). Geologic formations tend to be large, thus providing good opportunities for the remote sensing geologic scientist.

3. Commercial Satellite Systems

The spectral and spatial resolution characteristics of operational commercial, remote imaging satellite systems are summarized in Tables 1 through 3. Table 1 lists the characteristics of the two operational Landsat satellites, Landsat-5 and Landsat-7. Landsat-5 and Landsat-7 are multispectral sensors. Landsat-5 carries two sensor suites, namely the Multi-Spectral Scanner (MSS) and the improved Thematic Mapper (TM). Landsat-7 has as its main sensor the Enhanced Thematic Mapper (ETM). ETM is similar to TM, except that it has a 15 m resolution panchromatic band that is co-registered with the multispectral data so that the panchromatic and the multispectral images can be combined, enhancing the interpretation capability. Currently, the Landsat-7 ETM is not capable of producing full quality images because of the failure of the scan line corrector (SLC).

Table 1. Characteristics of operational Landsat sensors.

Satellite	Sensor	Band/wavelength (μm)	Resolution (m)	Operational period
Landsat-5	MSS	4/0.5-0.6 5/0.6-0.7 6/0.7-0.8 7/0.8-1.1	82 82 82 82	03/01/1984-present
	TM	1/0.45-0.52 2/0.52-0.60 3/0.63-0.69 4/0.76-0.90 5/1.55-1.75 6/10.4-12.5 7/2.08-2.35	30 30 30 30 30 120 30	
Landsat-7	ETM	1/0.45-0.52 2/0.52-0.60 3/0.63-0.69 4/0.76-0.90 5/1.55-1.75 6/10.4-12.5 7/2.08-2.35 panchromatic/ 0.50-0.90	30 30 30 30 30 150 30 15	04/15/1999-present

A substantial improvement in spatial resolution capabilities came with the launch on December 18, 1999 of the multispectral Advanced Spaceborne Thermal Emission and Reflection Radiometer (ASTER) satellite. The characteristics of the sensors onboard the ASTER satellite are summarized in Table 2. ASTER acquires images across 14 spectral bands with a swath width of 60 km and temporal resolution of 16 days. There are three

sensors onboard, collecting data in three different parts of the electromagnetic spectrum. The visible and near infrared (VNIR) sensor has an improved spatial resolution relative to Landsat-7 of 15 m and band 3 has a backward looking capability inclined at 27.6° from nadir, enabling stereo images. The short wave infrared (SWIR) sensor on ASTER acquires data in 6 spectral channels. The thermal infrared (TIR) sensor has spatial resolution of 90 m, which is superior to the 150 m resolution of band 6 in Landsat-7.

Table 2. Characteristics of ASTER satellite sensor.

Sensor	Band number	Spectral range (μm)	Spatial resolution (m)	Quantization levels
VNIR	1 2 3N 3B	0.52-0.60 0.63-0.69 0.78-0.86 0.78-0.86	15	8 bits
SWIR	4 5 6 7 8 9	1.60-1.70 2.145-2.185 2.185-2.225 2.235-2.285 2.295-2.365 2.360-2.430	30	8 bits
TIR	10 11 12 13 14	8.125-8.475 8.475-8.825 8.925-9.275 10.25-10.95 10.95-11.65	90	12 bits

A number of other commercial satellites have been launched which offer panchromatic and multispectral imaging capabilities. The characteristics of various commercial, operational satellite systems, namely SPOT-5, IRS-1C/D, Quickbird, Ikonos-2, and Early Bird-1, are summarized in Table 3.

Table 3. Characteristics of various commercial, operational satellite systems.

SPOT-5		IRS-1C/D		Quickbird		Ikonos-2		Early Bird-1	
Band/ Res. (m)	**λ (μm)**	**Band/ Res. (m)**	**λ (μm)**	**Band/ Res. (m)**	**λ (μm)**	**Band/ Res. (m)**	**λ (μm)**	**Band/ Res. (m)**	**λ (μm)**
B1/10	0.50-0.59	B1/23	0.52-0.59	B1/2.44	0.45-0.52	B1/4	0.45-0.52	B1/15	0.49-0.600
B2/10	0.61-0.68	B2/23	0.62-0.68	B2/2.44	0.52-0.60	B2/4	0.52-0.60		
B3/10	0.78-0.89	B3/23	0.77-0.86	B3/2.44	0.63-0.69	B3/4	0.63-0.69	B2/15	0.615-0.670
B4/20	1.58-1.75			B4/2.44	0.76-0.90	B4/4	0.76-0.90	B3/15	0.790-0.875
Panchromatic									
Pan/2.5 or 5	0.48-0.71	Pan/5.8	0.50-0.75	Pan/0.61	0.445-0.90	Pan/1	0.45-0.90	Pan/3	0.445-0.650

A significant improvement in spectral resolution capabilities was achieved with the launch of the Earth Observing-1 (EO-1) satellite on November 21, 2000. There are three basic earth imaging instruments on the EO-1 satellite, namely the Advanced Land Imager (ALI), Hyperion (hyperspectral imager), and Atmospheric Corrector (AC). The EO-1 ALI consists of a 15° Wide Field Telescope (WFT) and partially populated focal plane occupying 1/5th of the field-of-view, giving a ground swath width of 37 km. It provides seven multispectral bands from 0.43-2.35 μm with a spatial resolution of 30 m. Hyperion is a hyperspectral imager capable of resolving 220 spectral bands (from 0.4 to 2.5 μm) with 30 m ground resolution. The instrument can image a 7.5 km by 100 km land area per image, and provide detailed spectral mapping across all 220 channels with high (6%) radiometric accuracy. The AC is an imaging spectrometer covering the spectral range from 0.9 to 1.6 μm and a spatial resolution of 250 m. This instrument is specifically designed to measure atmospheric information to assist in analysis of the Hyperion and ALI imagery.

This page intentionally left blank.

4. Systematic Comparison of Uranium Mining and Milling to Other Types of Mineral Mining and Milling

4.1. Overview of Uranium Mining and Milling

4.1.1. Uranium Distribution, Ores and Minerals

In order to understand the processes used to mine and mill uranium, it is necessary to overview the chemical and geologic characteristics of uranium ores and associated host minerals. The average crustal abundance of uranium is 2.7 ppm, with significant variations among different types of host minerals [9]. Uranium is distributed in naturally occurring minerals in two oxidation states: U^{6+} (the oxidized uranyl ion) and U^{4+} (the reduced uranous ion). The uranyl ion tends to bestow a bright coloration, such as red, yellow, green, or orange, on the host mineral. Examples of common uranyl minerals include tyuyamunite ($Ca(UO_2)_2(VO_4)_2 \cdot 5\text{-}8H_2O$), autonite ($Ca(UO_2)_2(PO_4)_2 \cdot 10\text{-}12H_2O$), carnotite ($K_2(UO_2)_2(VO_4)_2 \cdot 1\text{-}3H_2O$), and uranophane ($Ca(UO_2)_2(SiO_3)_2(OH)_2 \cdot 5H_2O$). Minerals containing the uranous ion are typically black or brown. Examples of common uranous minerals include uraninite (UO_2), pitchblende (a crystalline variety of uraninite), and coffinite ($U(SiO_4)_{1-x}(OH)_{4x}$ [10].

Low grade cutoff values for the economic viability of uranium mining typically range from 0.05% to 0.3% U_3O_8. The low grade cutoff point is site specific and is dependent on the costs associated with mining the ore, feed requirements for processing the uranium at the mill, and the market price of uranium [11]. Economically viable uranium deposits, referred to as uranium ores, have been found in a wide range of host rocks and regions in the world. A majority of recoverable uranium deposits in the world occur in three geologic environments, conglomerates (19% of resources, e.g., Canada and South Africa), sandstones (44% of resources, e.g., United States, Australia, Niger, and Brazil), and veins (22% of resources, e.g., United States, Canada, Australia, France and Gabon) [10, 12]. In the case of the conglomerate type, the uranium host rock is an oligomictic conglomerate composed of quartz pebbles in a pyrite-rich, quartzitic matrix. The most abundant uranium ore minerals in conglomerate deposits are uraninite, brannerite, and uranothorite. In sandstone type deposits, the host rock is composed of sandstone (which is mainly quartz), pyrite, and carbonaceous material. In reduced zones, the dominant uranium ore minerals are pitchblende and coffinite. In oxidized zones, the most prominent uranium ore minerals are carnotite, tyuyamunite, and francevillate. The host rock for vein deposits is typically composed of quartz, carbonate, and hematite. The main uranium ore mineral in vein deposits is pitchblende. The wide geographic distribution of uranium and the fact that it is an essential part of a large number of minerals can be attributed to three factors: (1) uranium naturally occurs in two oxidation states, (2) the uranyl ion, UO_2^{2+}, is highly soluble, and (3) the uranyl ion and the tetravalent uranium ion, U^{4+}, are easily incorporated into many crystal structures.

4.1.2. Uranium Mining

Uranium is mined using one of three general techniques, namely surface (open pit) mining, underground mining, or solution (*in situ*) mining [11]. The mining method is selected based on the grade of the uranium ore and the geology and location of the deposit. Uranium ore deposits near the earth's surface are typically extracted using open pit mining techniques. In open pit mining, the soil and rock overlying the uranium deposit are first removed. Having exposed the ore body, the uranium ore is ripped with bulldozers or blasted with explosives, loaded into trucks, and transported to a stockpile. In contrast, in underground mining a shaft is drilled near the ore body and levels are extended from the main shaft to the ore. Ore and waste rock are transported to the surface by an elevator, conveyor belt, or train. Employing solution mining, a chemical leach solution is pumped down into an underground uranium ore deposit to dissolve the uranium, and the uranium solution is brought to the surface through recovery wells under suction pressure. Leaching solution is typically composed of carbonate/bicarbonate or dilute sulfuric acid. Solution mining is environmentally viable when the ore is underlain by a non-porous stratum to avoid the release of leaching solution outside the mining area.

4.1.3. Uranium Milling

Uranium milling is composed of five steps: (1) comminution, or crushing and grinding of the ore, (2) leaching of the uranium into solution, (3) separation of the uranium solution from the solid waste material or tailings, (4) concentration and purification of the uranium, and (5) precipitation and product preparation [10, 13].

4.1.3.1. Comminution

Comminution is performed in two stages, namely crushing and grinding [14]. The mined ore is crushed and ground in order to increase the exposed surface area of the uranium minerals, which increases the efficiency of later uranium extraction steps. The initial stage in the comminution process is crushing, which is a mechanical procedure focused on liberating the uranium minerals from the waste rock, or gangue. In the primary crushing stage, the ore is reduced from up to 1.5 m in diameter to 10-20 cm using heavy duty machines such as jaw crushers and gyratory crushers. Secondary crushing is performed using lighter duty machines, such as cone crushers and impact crushers, and produces a final crusher product which is typically between 0.5 cm and 2 cm in diameter. Grinding is the last stage of the comminution process where the diameter of ore is reduced through impact and abrasion. Grinding is generally performed in rotating, cylindrical steel vessels, called tumbling mills. Grinding can be performed either dry or in combination with water. The degree of grinding required is dependent on the ore hardness, the host rock mineralogy, and the type of leaching used, for example, acid or alkaline leaching. In the case of U.S. sandstone ores leached using acid, it is sufficient to grind the ore such that it passes a 28 mesh (590 μm) screen with 30 to 40 percent minus 200 mesh (75 μm) [10].

4.1.3.2. Leaching

Uranium can be leached or extracted into solution from the ore by acid or alkaline carbonate solutions [10, 13]. The mineral composition of the ore is the key factor dictating the process conditions required to generate the uranium solution, referred to as the pregnant leach liquor. Sulfuric acid solution is preferentially used for leaching, but the presence of carbonate minerals in the uranium ore such that more than 70-100 kg of sulfuric acid are consumed per tonne of ore may necessitate the use of a carbonate leaching solution.

Leaching can be performed in specialized tanks, in heaps, or *in situ* [11]. High grade uranium ores are generally leached in tanks, while lower grade ores are leached in heaps or *in situ*. Leaching in tanks typically takes from 4 to 24 hours, while heap leaching is less efficient and requires anywhere from days to weeks.

4.1.3.2.1. Acid Leaching

Sulfuric acid is preferred over other strong acids, such as hydrochloric acid and nitric acid, because it less expensive and less corrosive [10, 15]. Sulfuric acid can also be readily generated at remote mill sites through the oxidation of sulfur. Sulfuric acid reacts with hexavalent uranium to form the highly water soluble uranyl cation, thereby forming uranyl sulfate and complex ions:

$$UO_3 + 2H^+ \rightarrow UO_2^{2+} + H_2O$$

$$UO_2^{2+} + SO_4^{2-} \rightarrow UO_2SO_4$$

$$UO_2SO_4 + SO_4^{2-} \rightarrow UO_2(SO_4)_2^{2-}$$

$$UO_2(SO_4)_2^{2-} + SO_4^{2-} \rightarrow UO_2(SO_4)_3^{4-}.$$

If the uranium is present in the ore in the tetravalent oxidation state, it does not readily dissolve in sulfuric acid, and oxidation of the uranium to the hexavalent oxidation state is necessary:

$$UO_2 - 2e \rightarrow UO_2^{2+}.$$

Oxidation of the uranium is achieved in practice by the presence of ferric ions in the sulfuric acid solution:

$$UO_2 + 2Fe^{3+} \rightarrow UO_2^{2+} + 2Fe^{2+}.$$

The ferric ions, Fe^{3+}, must be renewed by oxidation of the ferrous ion, Fe^{2+}. Manganese dioxide, MnO_2, and sodium chlorate, $NaClO_3$, are two oxidizing agents commonly used in uranium milling to regenerate the required ferric ions:

$$2Fe^{2+} + MnO_2 + 4H^+ \rightarrow 2Fe^{3+} + Mn^{2+} + 2H_2O$$

$$6Fe^{2+} + NaClO_3 + 6H^+ \rightarrow 6Fe^{3+} + NaCl + 3H_2O.$$

Typically, 1 to 3 kg of MnO_2 is required per tonne of uranium ore processed in the United States and Australia. Up to 1.5 kg $NaClO_3$ per tonne of ore is required in uranium mills in the United States and Canada.

Efforts are made to minimize the consumption of acid by gangue minerals in the ore. Carbonate, calcite, dolomite, magnesite, and siderite readily consume sulfuric acid at low temperature and low acid concentration, reducing leaching efficiency. As an example, carbonate consumes sulfuric acid according to the following chemical reaction:

$$CaCO_3 + H_2SO_4 \rightarrow CaSO_4 + CO_2 + H_2O$$

Generally, uranium mills consume acid in amounts of 20-50 kg/tonne of ore processed.

4.1.3.2.2. Alkaline Leaching

Oxidized uranium minerals such as carnotite are readily soluble in carbonate solutions [10, 13, 16]. In carbonate leach solutions, oxidized uranium minerals react with the carbonate ion, CO_3^{2-}, to form the soluble uranyl tricarbonate ion. As an example, the hexavalent carnotite ion interacts with carbonate ions according to the following chemical reaction :

$$K_2(UO_2)_2(VO_4)_2 \cdot 3H_2O + 6CO_3^{2-} \rightarrow 2K^+ + 2UO_2(CO_3)_3^{4-} + 2VO_3^- + 4OH^- + H_2O.$$

On average, uranium mills consume 30 to 60 g of Na_2CO_3 per liter of leach solution and 5-15 g/liter of $NaHCO_3$, with the pH maintained between 9 and 10.5.

Tetravalent uranium minerals typically need to be leached for long time periods at high temperature and under oxidizing conditions to achieve suitable dissolution. In practice, tetravalent uranium minerals are oxidized through the addition of molecular oxygen to the carbonate solution. As an example, the oxidation of uraninite and subsequent dissolution of uranium can be represented by the following chemical equations:

$$2UO_2 + O_2 \rightarrow 2UO_3$$

$$2UO_3 + 6CO_3^{2-} + 2H_2O \rightarrow 2UO_2(CO_3)_3^{4-} + 4OH^-.$$

4.1.3.3. Solid-Liquid Separation

With the exception of the resin-in-pulp (RIP) procedure, all methods of uranium recovery require a solid-liquid separation step after leaching [13]. The pregnant leach liquor is isolated from the solid waste using thickeners and filters [14]. Sand-sized particles and slimes are removed and washed with clean water or barren process water. Flocculants can be added to prompt the settling of suspended particles. The solids, composed of sands and slimes, are washed a final time and pumped to a tailings pond or tailings dam for disposal [14]. Once separated from the solids, the pregnant leach liquor enters an ion exchange or solvent extraction circuit.

4.1.3.4. Concentration and Purification

The pregnant leach liquor generated by acid leaching is dilute and impure, and additional concentration and purification steps are required [10]. Alkaline leaching may generate a uranium solution of sufficient quality that an acceptable product can be precipitated directly from the leach liquor.

Ion exchange and solvent extraction are the two principal methods used for concentration and purification. Ion exchange can be applied to pulps and clarified solution from both alkaline and acid leaching. Solvent extraction is applicable to clarified acid leach solutions. A brief review of the chemistry involved in the ion exchange and solvent extraction processes is given below.

4.1.3.4.1. Ion Exchange Purification

Ion exchange utilizes strong base, quaternary-ammonium type resins, in the form of rigid, spherical beads, to purify the uranium. Conventionally, the resin is held in a column. Assuming that the resin is initially in the chloride form, the principal chemical reaction can be represented as follows [10]:

$$4R_4NCl + UO_2(SO_4)_3^{4-} \rightarrow (R_4N)_4UO_2(SO_4)_3 + 4Cl^-$$

The most prevalent uranyl species in the leach liquor feed solution is $UO_2(SO_4)_2^{2-}$, with UO_2^{2+}, UO_2SO_4, $UO_2 \cdot OH \cdot SO_4^-$, and $UO_2(SO_4)_3^{4-}$ also present. The concentration of uranium in the leach liquor feed solution is typically between 0.5 to 1.5 g/L. Having loaded the resin column with uranium, the uranium is eluted from the column with a 1 M sodium chloride/0.05 M sulfuric acid solution, thereby reversing the reaction given above.

4.1.3.4.2. Solvent Extraction Purification

Solvent extraction is a process that concentrates uranium by utilizing the immiscible properties of aqueous and organic solvents and by manipulating the solubility of uranium in the two solvents. Solvent extraction is carried out in two stages: (a) uranium is transferred from an aqueous phase to an organic phase, and (b) uranium is transferred from this organic phase to a new aqueous phase [13].

In the first stage of solvent extraction, uranium is selectively transferred from the aqueous pregnant leach liquor to an organic solvent. The two types of organic solvents used in uranium mills are tertiary amines, referred to as the AMEX process, and alkylphosphoric acids, referred to as the DAPEX process. The amine or alkylphosphate is diluted to approximately 5% by volume by an inert organic such as kerosene, and up to 5% of a modifying agent is added [10]. Uranium is selectively transferred from the aqueous pregnant leach liquor to the organic tertiary amine solution according to the following chemical reaction:

$$4R_3NHCl + UO_2(SO_4)_3^{4-} \rightarrow (R_3NH)_4UO_2(SO_4)_3 + 4Cl^-.$$

Uranium is selectively transferred from the aqueous pregnant leach liquor to the organic alkylphosphoric acid solution according to a different reaction:

$$2(HR_2PO_4)_2 + UO_2^{2+} \rightarrow (R_2PO_4HR_2PO_4)_2UO_2 + 2H^+.$$

Following this first extraction step, the concentration of uranium in the organic phase is typically between 3.5 to 6 g U_3O_8/L, with only 0.002 g U_3O_8/L remaining in the barren, aqueous raffinate [10].

In the second stage of the solvent extraction process, the uranium is stripped from the organic phase and transferred to an aqueous phase, referred to as the loaded strip liquor [13]. Uranium can be stripped from amine solvents using a variety of reagents, including sodium or ammonium chloride, ammonium nitrate, sodium carbonate, and ammonium sulfate. Alkyl phosphate solvents are commonly stripped with aqueous sodium carbonate. Following stripping, the concentration of uranium in aqueous solution can range between 15 and 50 g U_3O_8/L [10, 13].

4.1.3.5. Precipitation and Product Preparation

A solid uranium product is recovered from solution by chemical precipitation [10, 13]. In processing clarified alkaline leach liquors, uranium is recovered through the addition of sodium hydroxide, which neutralizes the bicarbonate ion and precipitates uranium as disodium urinate. In this process, the pH is raised above 12. In plants that utilize acid leaching, uranium is precipitated from the loaded strip liquor by neutralization with a base such as lime, caustic soda, magnesia, or ammonia. To produce the uranium precipitate known as yellowcake, the pH of the loaded strip liquor is adjusted to 7.0.

Following precipitation, the yellowcake is dewatered using filters and centrifugation. High temperature drying of the yellowcake at temperatures between 400 and 800ºC is also commonly employed. The dried yellowcake is crushed, passed through a screen with 0.25 inch openings, and packed in 55 gallon drums.

4.1.3.6. Alternative Uranium Processing Methods

Several alternative uranium processing methods, such as the Excer process, the Winlo process, the Eluex process, bacterial leaching, and heap leaching, have been developed and implemented. Interested readers can refer to [10] for a discussion of these alternative uranium processing methods.

4.2. Ranger Uranium Mine and Mill

As is evident in Section 4.1, a variety of processes can be used in the mining and milling of uranium. In this report, we focus our attention on the Ranger uranium mine and mill in Australia and document the potential observables associated with uranium mining and milling at the Ranger site [7]. An advantage of using Ranger as an example is that it is a well-known site with a large body of open literature information.

Located in a monsoonal part of Northern Australia, Ranger is an open pit mine. The removal of rock from pit #1 has been completed, and pit #3 is currently being mined. Milling is performed at the Ranger site using sulfuric acid leaching and solvent extraction. Uranium production at Ranger in calendar year 2004 was 5137 tonnes of U_3O_8.

The mining and milling process at Ranger is composed of seven steps: (1) mining, (2) crushing and grinding, (3) leaching, (4) solid-liquid separation, (5) solvent extraction, (6) precipitation and drying, and (7) tailings neutralization and disposal [7]. In step 1, rock is extracted from the open pit mine and loaded into a truck. The main host to the uranium mineralization is a quartz-chlorite schist in the upper mine sequence [17, 18]. The main uranium ore mineral is uraninite. Each truck load of ore removed from the open pit mine is sorted using a radiometric discriminator. Based on this radiometric measurement, which is indicative of the percentage of uranium in the rock, the material is delivered to a waste pile, to a particular stockpile, or directly to the primary crusher. The ore grade at Ranger is 0.30% U_3O_8. In step 2, the crushing and grinding process, the uranium ore is reduced to a fine size (80% passing 0.174 mm) in order to increase leaching efficiency. Aqueous solution is added to the ore to create a slurry. In step 3, the uranium ore slurry is leached with sulfuric acid in a series of ten air-agitated pachuca tanks. Sulfuric acid is produced on site at an acid plant using stockpiled sulfur. Pyrolusite, a form of manganese dioxide, is added as an oxidant to increase leaching efficiency. In step 4, solid-liquid separation, the pregnant leach liquor, containing a vast majority of the uranium, is separated from the solid waste material or tailings. Solid-liquid separation is achieved through the use of counter current decantation thickener tanks, a clarifying thickener tank, and sand filters. In step 5, solvent extraction, uranium is first extracted from the aqueous pregnant leach liquor in a series of four mixer-settler units with an organic kerosene phase containing an amine which selectively complexes the uranium. The uranium-loaded organic solution is then passed to another series of four smaller mixer-settler units. The uranium is transferred to an aqueous phase through a change in pH achieved through the addition of ammonia. In step 6, precipitation and drying, ammonium diuranate is precipitated as yellowcake from the loaded strip solution by raising the pH with ammonia. The precipitate is centrifuged and calcined in a multihearth furnace. Finally, in step 7, tailings neutralization and disposal, the pH of the acidic tailings is increased to 7.5 by mixing the solid waste material with lime in air-agitated pachuca tanks, and the tailings are pumped to a storage area. Until 1996 tailings from the treatment plant were placed in an engineered dam, but they are now being deposited into the worked out pit #1.

Figure 3 depicts a 61 cm spatial resolution Quickbird satellite image of the Ranger mine and mill. Different operational elements of the Ranger mine and mill are labeled on Figure 3. The 61 cm spatial resolution of the Quickbird sensor allows one to zoom in on particular elements within the Ranger site and view individual structures. Figure 4 shows a close-up view of the Ranger mill area, captured using the Quickbird sensor. The various elements of the Ranger milling operation, including the acid plant, the sulfur stockpile, the air-agitated pachuca tanks, the counter current decantation thickener tanks, the clarifying thickener tank, and the mixer-settler units, are labeled on Figure 4. In contrast, Figure 5 shows a 30 m spatial resolution Hyperion satellite image of the Ranger mine and mill. Large structures at the Ranger site, such as the tailings ponds and the open pit mine, can be seen in the Hyperion image. However, smaller structures in the mill area, such as the neutral thickener tank, the pachuca tanks, the thickener (counter current decantation) tanks, and the mixer-settler units, cannot be seen in the Hyperion image.

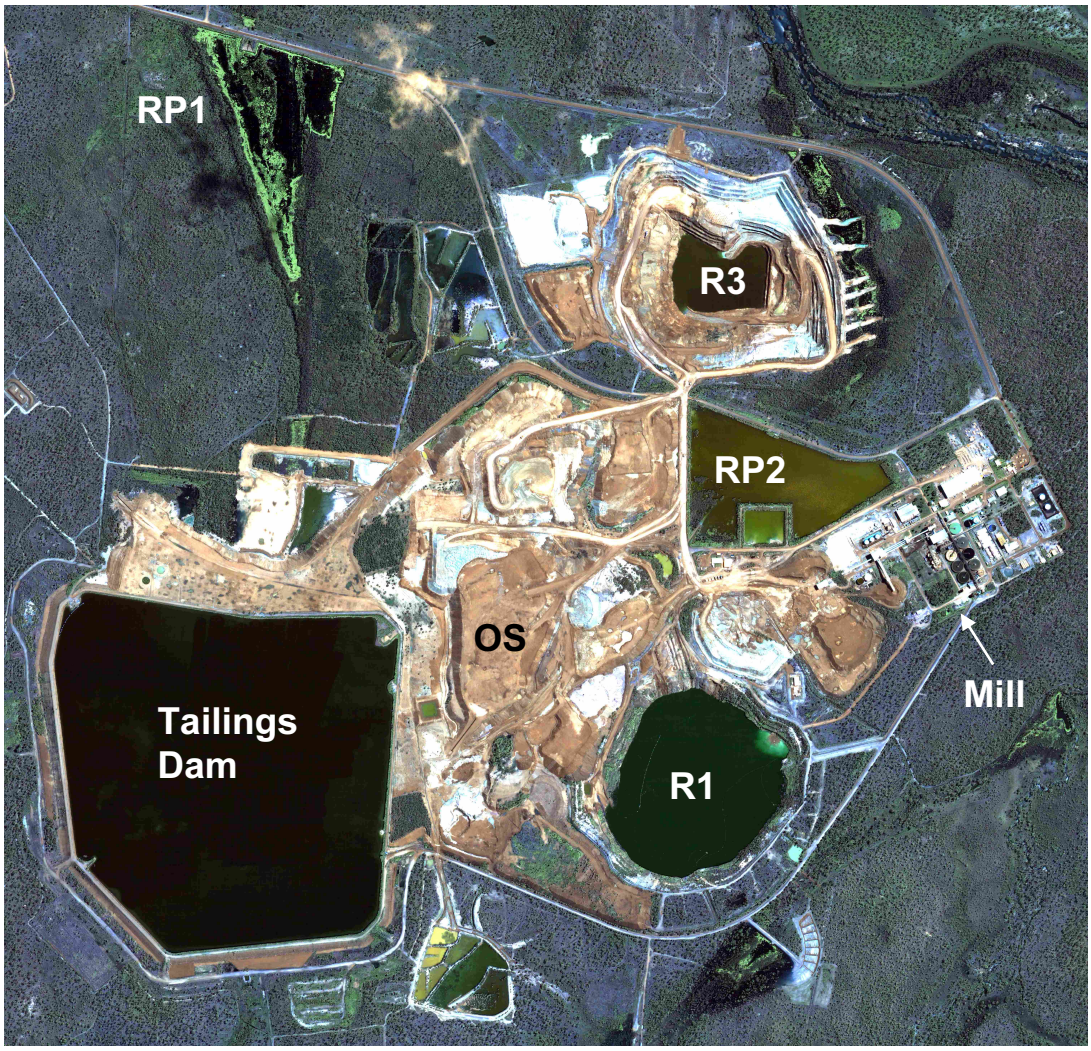

Figure 3. RGB pan-sharpened, 61 cm resolution Quickbird satellite image of the Ranger mine and mill. (RP1 = Retention Pond 1, RP2 = Retention Pond 2, R1 = Ranger #1 Pit, R3 = Ranger #3 Open Pit Mine, OS = Ore Stockpile)

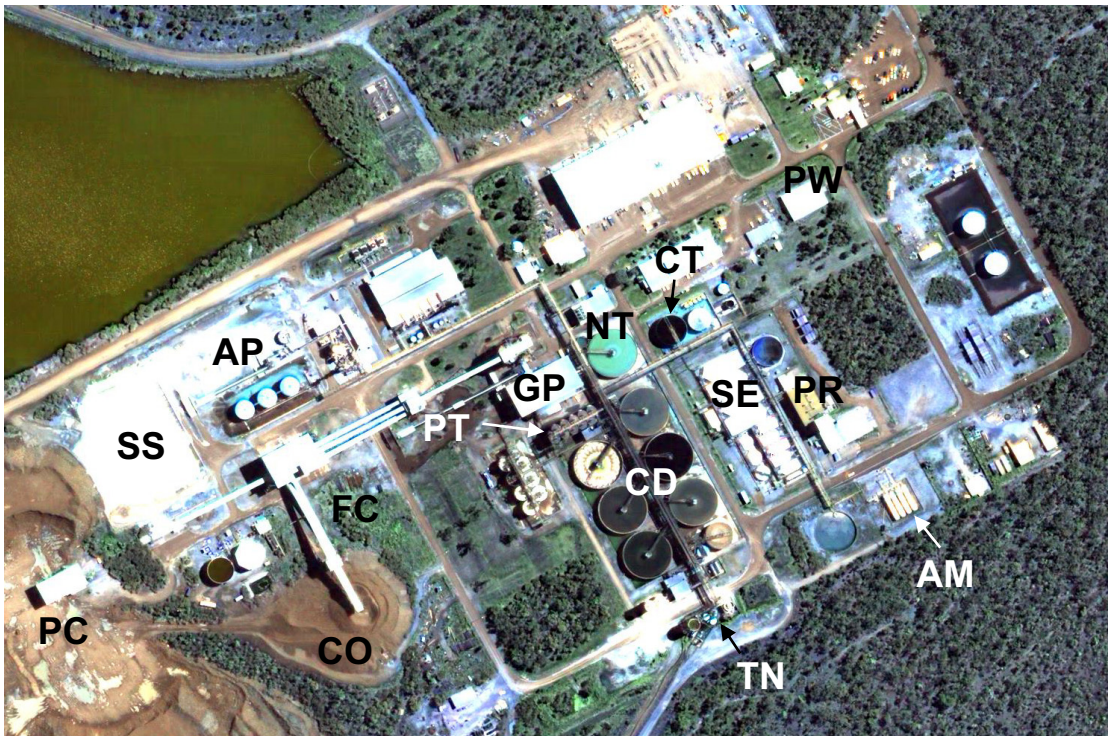

Figure 4. RGB pan-sharpened, 61 cm resolution Quickbird satellite image of Ranger mill. (SS = Sulfur Stockpile, PC = Primary Crusher, FC = Fine Crusher, CO = Coarse Ore Stockpile, NT = Neutral Thickener, AP = Acid Plant, PT = Pachuca Leaching Tanks, GP = Grinding and Pyrolusite, CD = Counter Current Decantation Thickeners, CT = Clarifying Thickener, SE = Solvent Extraction, PR = Precipitation, AM = Ammonia Tanks, PW = Product Warehouse, TN = Tailings Neutralization)

Figure 5. RBG 30 m resolution Hyperion satellite image of Ranger mine and mill.

Table 4 lists potential observables associated with each of the seven primary mining and milling steps employed at Ranger and also designates whether these observables are unique to uranium mining and milling. In Table 4, 'Exposed' refers to whether the observables are contained in covered or uncovered structures.

Table 4. Summary of potential observables at Ranger mine and mill.

Table 4(a). Uranium mining.

Target	Potential Observables	Size	Exposed	Unique to uranium mine/mill	Comments	References
Open pit mine	Ore composition – Mg chlorite, quartz, sericite, 0-0.5% U minerals (primarily uraninite)	437000 m^2	Yes	No	Uranium and other minerals can occur in same host rock	[17, 18]
Ore stockpile	Ore composition – Mg chlorite, quartz, sericite, 0.2-0.5% U minerals		Yes	No		[17, 18]
Gangue stockpile	Composition – Mg chlorite, quartz, sericite		Yes	No		[17, 18]
Discriminator station	Discriminator building	5 m by 8 m	Yes	Yes (difficult to distinguish from other buildings)	No unique spectrum – dependent on building material	[4, 7]
Retention pond 2	Runoff from mine pit, ore stockpiles, and mill site	164000 m^2	Yes	No		[19]
Retention pond 1	Runoff from waste rock (U < 0.02%)		Yes	No		[19, 20]

Table 4(b). Uranium milling: crushing and grinding circuit.

Target	Potential Observables	Size	Exposed	Unique to uranium mine/mill	Comments	References
Primary crusher	Primary crusher building	700 m^2	Yes	No	No unique spectrum – dependent on building material	[4, 7]
Fine ore crushing station	Crushing station structure	1230 m^2	Yes	No	No unique spectrum – dependent on building material	[4, 7]
Coarse ore stockpile	Ore composition – Mg chlorite, quartz, sericite, 0.2% U minerals	7780 m^2	Yes	No		[4, 7]

Table 4(c). Uranium milling: leaching.

Target	Potential Observables	Size	Exposed	Unique to uranium mine/mill	Comments	References
Neutral thickener	Surface water containing dissolved solids, flocculant	39 m diameter tank	Yes (occurs in open tank)	No	Used to remove excess water from ground ore	[4, 7]
Leaching	1. Sulfuric acid, 2. oxidant (manganese dioxide, MnO_2), 3. pachuca tanks	Ten 7 m diameter pachucas	1. No, 2. No, 3. Yes (pachuca tanks are visible, contents are not)	No	Sulfuric acid leaching is common mineral milling procedure	[7, 10]
Sulfur stockpile	Elemental sulfur	9100 m^2	Yes	No (but indicative of acid leaching)	Sulfur used to produce sulfuric acid for leaching	[4]
Sulfuric acid plant	Sulfuric acid, sulfur dioxide		Yes	No (sulfuric acid used to leach other minerals)	Sulfuric acid can be produced as by-product of copper sulfide ore milling	[4]
Sulfuric acid tanks	Sulfuric acid	Three 15 m diameter tanks	No (sulfuric acid stored in closed tanks)	No	Sulfuric acid can be produced as by-product of copper sulfide ore milling	[4]
Pyrolusite stockpile	Manganese dioxide (MnO_2)	12 m diameter tank	Unknown	No	Manganese dioxide used as oxidant in leaching of U. Consumption of MnO_2 usually 1-3 kg/tonne in USA and Australia. In electrolytic zinc production, MnO_2 used to purify leach solution by oxidizing iron.	[4, 7, 10, 21]

Table 4(d). Uranium milling: solid-liquid separation.

Target	Potential Observables	Size	Exposed	Unique to uranium mine/mill	Comments	References
Thickeners (counter current decantation)	1. Pregnant leach liquor (PLL) (increased concentration of U), 2. tailings	Six 39 m diameter tanks	Yes	1. Yes (PLL is unique indicator of uranium milling), 2. No	Pregnant leach liquor contains 0.5-1.5 g/L U_3O_8. CCD thickeners are ubiquitous and not unique to U milling. U complexes that exist in acid sulfate solutions include UO_2SO_4, $UO_2(SO_4)_2^{2-}$, $UO_2(SO_4)_3^{4-}$, and $UO_2(HSO_4)_2$.	[4, 7, 22, 23]
Clarifying thickener	PLL	24 m diameter tank	Yes	Yes (PLL is unique indicator of uranium milling)	The clarifying thickener is used to remove suspended solids. Clarifying thickeners are ubiquitous and not unique to U milling.	[7, 22]
Sand Filters	PLL	18 m diameter tank	Unknown	Yes (PLL is unique indicator of uranium milling)	Sand filters are not unique to U milling.	[4, 7, 22]

Table 4(e). Uranium milling: solvent extraction.

Target	Potential Observables	Size	Exposed	Unique to uranium mine/mill	Comments	References
Four extraction mixer-settler units	1. Kerosene, 2. trialkylamine (3.5% in kerosene), 3. isodecanol (1.0% in kerosene), 4. concentrated U	Four 420 m^2 units	No	1. No, 2. No, 3. No, 4. Yes	Kerosene is used as the organic phase in many mineral solvent extraction operations	[4, 7, 10]
Four smaller strip mixer-settlers	1. Ammonia, 2. concentrated U	Four 110 m^2 units	No	1. No, 2. Yes	Strip solution at typical U mill normally contains 25 to 40 g/L U_3O_8	[7, 24]
Ammonia storage tanks	Ammonia	Four 93 m^2 tanks	No (may be able to detect leaks)	No	Ammonia stored in closed tanks, but gas leaks may be detectable	[4]

Table 4(f). Uranium milling: precipitation and drying.

Target	Potential Observables	Size	Exposed	Unique to uranium mine/mill	Comments	References
Precipitation tank	1. Ammonia, 2. yellowcake		No	1. No, 2. Yes	Ammonia and/or ammoniacal salts are used in leaching of oxide ores of nickel, manganese nodules, and sulfide concentrates of copper, nickel, and cobalt.	[7, 25]
Ammonium diuranate thickener	Yellowcake		No	Yes	Excess water removed	[7]
Centrifuge	Yellowcake		No	Yes	Centrifuges are not unique to uranium milling (commonly used in dewatering).	[7, 14]
Multihearth furnace (calciner)	Heat (800ºC)		No	No		[7]
Yellowcake storage	Steel drums		No	Yes		[4, 7]

Table 4(g). Uranium milling: tailings neutralization and disposal.

Target	Potential Observables	Size	Exposed	Unique to uranium mine/mill	Comments	References
Neutralization pachucas	1. Tailings, 2. lime		Unknown	1. No, 2. No	Lime is used to neutralize acidic tailings	[7]
Tailings ponds (tailings dam and Ranger #1 pit)	1. Species dissolved in water – sulfate, manganese, traces of uranium; 2. saturated tailings	Tailings dam is 1 km^2; #1 pit is 260000 m^2	Yes (tailings largely covered by water)	1. No, 2. No	Tailings ponds are used to contain excess water during the wet season. The concentrations of key analytes in process water (pit #1) are: 20 g/L SO_4, 1.63 g/L Mn, and 24 ppm U. The main forms of uranium in solution include UO_2^{2+}, UO_2SO_4, $UO_2(SO_4)_2^{2-}$, and UO_2OH^+. May be able to correlate composition of process water to chemical processes used in mill.	[7, 26, 27]

4.3. Copper Mining and Milling

As is the case for uranium ore, copper ore is typically mined using either underground or open pit mining [28]. *In situ* or solution mining is another alternative for extracting copper from the ore.

Different milling procedures are employed for copper occurring in sulfide and oxide form [14, 28]. Copper ore containing copper sulfide minerals is crushed and ground to aid in copper recovery. The copper sulfide minerals are recovered by a floatation process. Employing floatation, a slurry is formed by mixing the finely ground ore with water. Chemical reagents that coat the copper sulfide minerals are added to the slurry. The coated copper sulfide minerals are captured by rising air bubbles and these air bubbles float to the surface. The froth is skimmed off and dried. The dried material, called copper concentrate, contains approximately 30% copper, 27% iron, and 33% sulfur. In a process referred to as smelting, the copper concentrate is fed to a series of furnaces where the contaminants are removed and 99% pure copper is obtained.

In contrast, copper ore containing copper oxide minerals are milled using leaching and electrowinning [14, 28]. Copper leaching is typically performed using sulfuric acid. *In situ* leaching, heap leaching of unground ore, and vat leaching of crushed and finely ground ore can all be utilized. The copper solution is concentrated at a solvent extraction plant using organic chemicals. The electrolyte solution generated through solvent extraction is transferred to an electrowinning process where copper is plated out as a 99.99% pure copper cathode.

Uranium mines and mills share many elements and processes with other types of mineral mines and mills, most notably copper [24, 25]. Due to the close similarity between Ranger and copper mining and milling operations, such as the Nchanga copper tailings leach plant in Zambia [29], distinguishing between uranium and copper mining and milling activity can be problematic.

To document the similarity between Ranger and copper mining and milling, Table 5 lists the steps and observables associated with copper milling at the Nchanga copper tailings leach plant in Zambia [29]. The milling process at Nchanga is composed of six steps: (1) materials handling and preparation, (2) acid leaching, (3) solid-liquid separation, (4) solvent extraction, (5) electrowinning, and (6) residue neutralization and disposal. Development of the Nchanga tailings leach plant was motivated by the fact that the floatation tailings from the Chingola Concentrator contain approximately 0.4% acid soluble copper occurring in oxide form. In step 1, materials handling and preparation, the floatation tailings are reclaimed from a tailings dam by hydraulic and low pressure erosion lines, screened to remove waste material, and pumped at a density of 40% solids to the leaching plant. In step 2, acid leaching, the slurry is combined with sulfuric acid in pachuca tanks and the copper oxide minerals are brought into solution. In step 3, solid-liquid separation, the copper pregnant leach liquor is separated from the solid waste by washing in four 76 m diameter counter current decantation thickeners, followed by clarification in pressure sand filters. In step 4, solvent extraction, solution concentration and purification is achieved in four parallel solvent extraction streams. Each solvent

extraction stream is composed of three extraction and two strip stages. In step 5, electrowinning, the copper electrolyte solution produced by solvent extraction is pumped to the electrowinning tank house and copper is plated onto starter sheet cathodes. Finally, in step 6, residue neutralization and disposal, the washed solid waste from the thickeners is neutralized with lime in pachucas, and then pumped to a tailings dam. With the exception of the electrowinning step, significant parallels are noted between the milling practices at Nchanga and at Ranger.

Table 5. Summary of potential observables at Nchanga copper tailings leach plant.

Table 5(a). Materials handling and preparation.

Target	Potential Observables	Size	Exposed	Comments
Current tailings from Chingola Concentrator	Tailings (0.4% acid soluble copper)		Yes	Flotation tailings contain 0.4% acid soluble copper
Reclaimed material	Reclaimed material		Yes	
Leach residue	Leach residue		Yes	Routed directly to leach section

Table 5(b). Copper leaching.

Target	Potential Observables	Size	Exposed	Comments
Pre-leach thickener (excess water removed from reprocessed tailings)	Surface water containing dissolved solids, flocculant		Yes	
Leaching	Sulfuric acid	Twelve leach pachucas (10.6 m diameter)	No	Leaching carried out in two stages in air agitated pachucas
Sulfuric acid tanks	Sulfuric acid		No	Sulfuric acid produced as by-product of copper sulfide ore milling

Table 5(c). Solid-liquid separation.

Target	Potential Observables	Size	Exposed	Comments
Thickeners (counter current decantation)	Pregnant leach liquor, tailings, flocculant	Four 76 m diameter tanks	Yes	Pregnant leach liquor contains increased concentration of copper (2.3-2.5 g/L copper)
Pressure sand filters	Pregnant solution		Unknown	

Table 5(d). Solvent extraction.

Target	Potential Observables	Size	Exposed	Comments
Extraction mixer-settler units	LIX 64N extractant (1%), organic Napoleum 470 diluent, concentrated Cu		Unknown	
Strip mixer-settler units	Advance electrolyte (50 g/L Cu)		Unknown	
LIX yard	LIX		Unknown	

Table 5(e). Electrowinning.

Target	Potential Observables	Size	Exposed	Comments
Electrowinning tank house	Copper starter sheet cathodes, cobalt sulfate, salt, flocculant		Unknown	

Table 5(f). Residue neutralization and disposal.

Target	Potential Observables	Size	Exposed	Comments
Three neutralization pachucas	Tailings, lime		Unknown	Acidic washed residue from thickeners is neutralized with lime
Lime storage	Lime		Unknown	Lime used to neutralize tailings
Tailings dam	Tailings, species dissolved in water		Yes	

4.4. Other Minerals Leached Using Sulfuric Acid

In addition to uranium and copper, zinc, vanadium, rare earth minerals (monazite and $(Ce,La,Y,Th)(PO_4)$), phosphorus, and manganese are leached using sulfuric acid (p. 93 in [25]; pp. 132-133, 137-138 in [24]; [30]). Vanadium is often milled in conjunction with uranium. In the case of phosphorus, phosphate rock (mainly $Ca_3(PO_4)_2$) is leached with sulfuric acid to produce phosphoric acid and calcium sulfate residue. A very limited amount of manganese is produced using sulfuric acid leaching. A summary of the milling steps for zinc, vanadium, rare earth minerals, and phosphorus following sulfuric acid leaching is provided in Table 6. Table 6 also lists potential observables associated with each of these milling steps.

Table 6. Summary of milling steps and potential observables for zinc, vanadium, rare earth minerals, and phosphorus following sulfuric acid leaching.

Mineral	Steps	Potential Observables
Zinc (Zn)	1. Solid-liquid separation 2. Solution purification and concentration 3. Recovery from solution by electrowinning	1. Pregnant Zn leach liquor (20-30 g/L Zn) 2. Concentrated Zn liquor (100 g/L Zn) 3. Zn cathode sheets
Vanadium (V)	1. Solid-liquid separation 2. Solution purification and concentration 3. Recovery from solution by precipitation	1. Pregnant V leach liquor (3 g/L V_2O_5) 2. Concentrated V liquor (60 g/L V) 3. Ammonia
Rare Earth Minerals	1. Solid-liquid separation 2. Recovery from solution by selective precipitation	1. Monazite sulfate leach liquor 2. Ammonium hydroxide
Phosphorus (P)	1. Solid-liquid separation 2. Concentration	1. Phosphoric acid, calcium sulfate 2. Concentrated phosphoric acid, P_2O_5

4.5. Decision Tree for Differentiating Uranium Mines and Mills from Other Types of Mineral Mines and Mills

Differentiating uranium mining and milling operations from other types of mineral mines and mills is a difficult task. This is attributable to the fact that uranium mines and mills share many common processes and potential observables with other types of mineral mines and mills. In inspecting Table 4, which summarizes the steps involved in uranium mining and milling at the Ranger site, it is apparent that there are very few potential observables that are unique to uranium mining and milling. Due to the limited number of unique, potential observables associated with uranium mining and milling, it may be necessary to utilize multiple, non-unique observables in making a conclusion regarding the type of mineral being extracted at a mining and milling site. The information contained in multiple, non-unique observables can be used to narrow down the number of possible mineral mining and milling activities carried out at a particular site, and

potentially even unambiguously identify the type of mineral extracted at that site. Based on our literature research of uranium mining and milling [10, 13, 23] and research of mining and milling practices used for other types of minerals [24, 25, 30, 31], we have developed a decision tree which utilizes the information contained in one or more observables to determine whether uranium is possibly being mined and/or milled at a given site. The decision tree is presented in Figures 6(a), 6(b) and 6(c). Figure 6(a) focuses on observables associated with the mined ore to assess the possibility of uranium mining activity at a given site. Figure 6(b) focuses on observables associated with the leaching process to determine if uranium milling is being carried out at a given site. Figure 6(c) employs a series of observables to differentiate between minerals that are leached using sulfuric acid. The decision tree is color-coded. Points in the decision tree in which uranium mining or milling at the site in question can be definitively confirmed or excluded are highlighted in red. Points in the decision tree in which the number of possible minerals being mined or milled at the site can be narrowed down are highlighted in blue.

The application of the decision tree can be demonstrated through an example. Suppose at a given mining and milling site the following observables are identified: (a) the ore host rock is composed of quartz pebble conglomerates, (b) pachuca tanks are used in the mill, (c) sulfuric acid is used in the milling operation, and (d) pyrolusite is used as a leaching agent. The process is initiated by consulting the ore assessment portion of the decision tree, shown in Figure 6(a). Unique U features were not identified in the ore spectrum, preventing one from immediately assessing this to be a uranium mine. The identification of quartz pebble conglomerates in the host rock is an indicator of uranium mining. However, more evidence must be assembled. Next, the section of the decision tree focused on observables associated with leaching, shown in Figure 6(b), is consulted. The identification of pachuca tanks, sulfuric acid, and pyrolusite at the mill site are all indicative of leaching. The type of leaching used at the mill site is acid leaching, as can be deduced from the presence of sulfuric acid. The fact that sulfuric acid is used at the mill narrows the possible mineral candidates to uranium, copper, zinc, manganese, vanadium, the rare earths, and phosphorus. One is then directed to Figure 6(c), the portion of the decision tree that uses multiple observables to differentiate between minerals that are leached using sulfuric acid. The identification of pyrolusite as a leaching agent at the site further narrows the possible mineral candidates to uranium and zinc. The lack of additional observables at the mill site prevents any further deductions regarding the type of mining and milling carried out at the site.

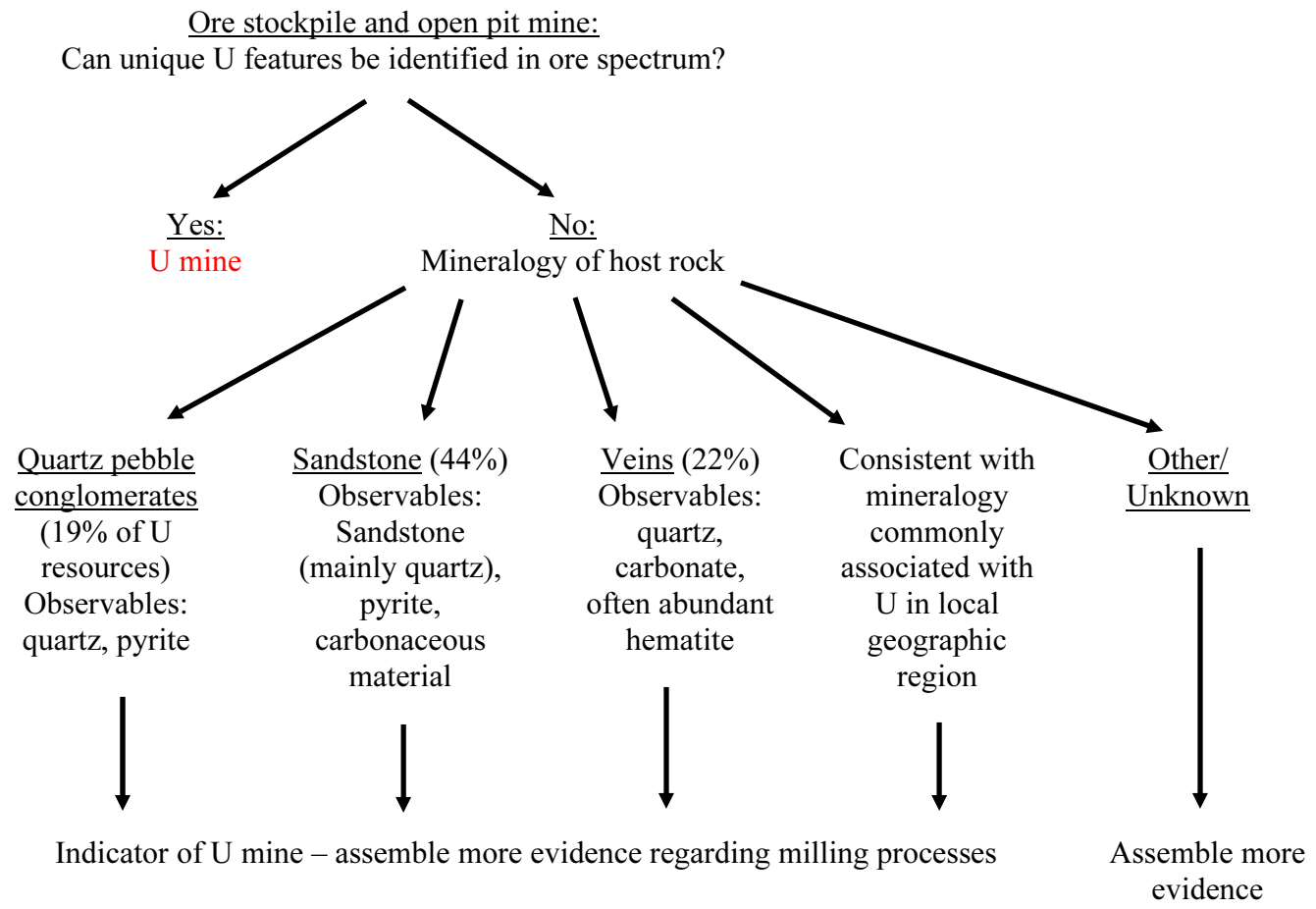

Figure 6 (a). Decision tree – ore assessment.

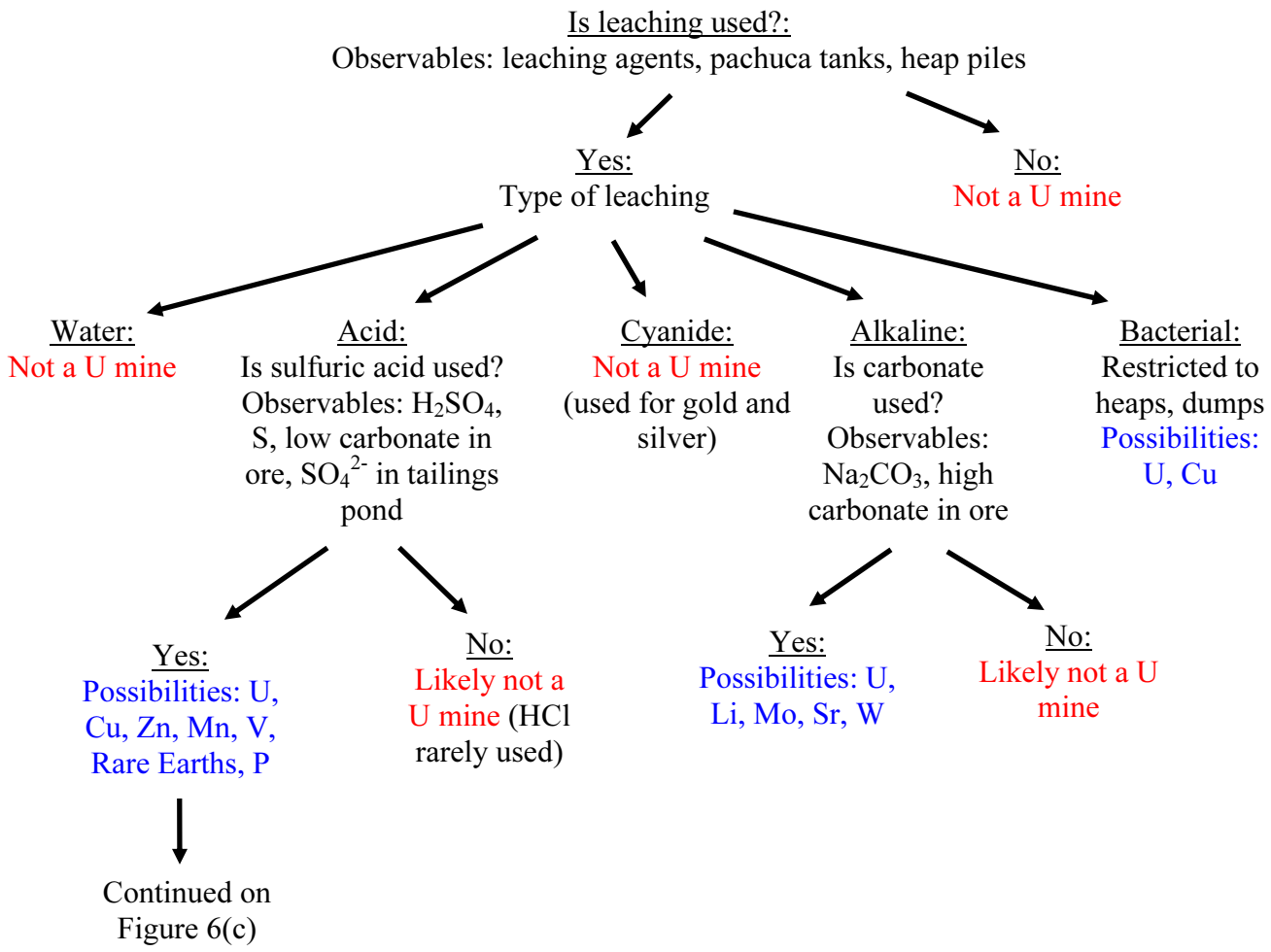

Figure 6(b). Decision tree – leaching.

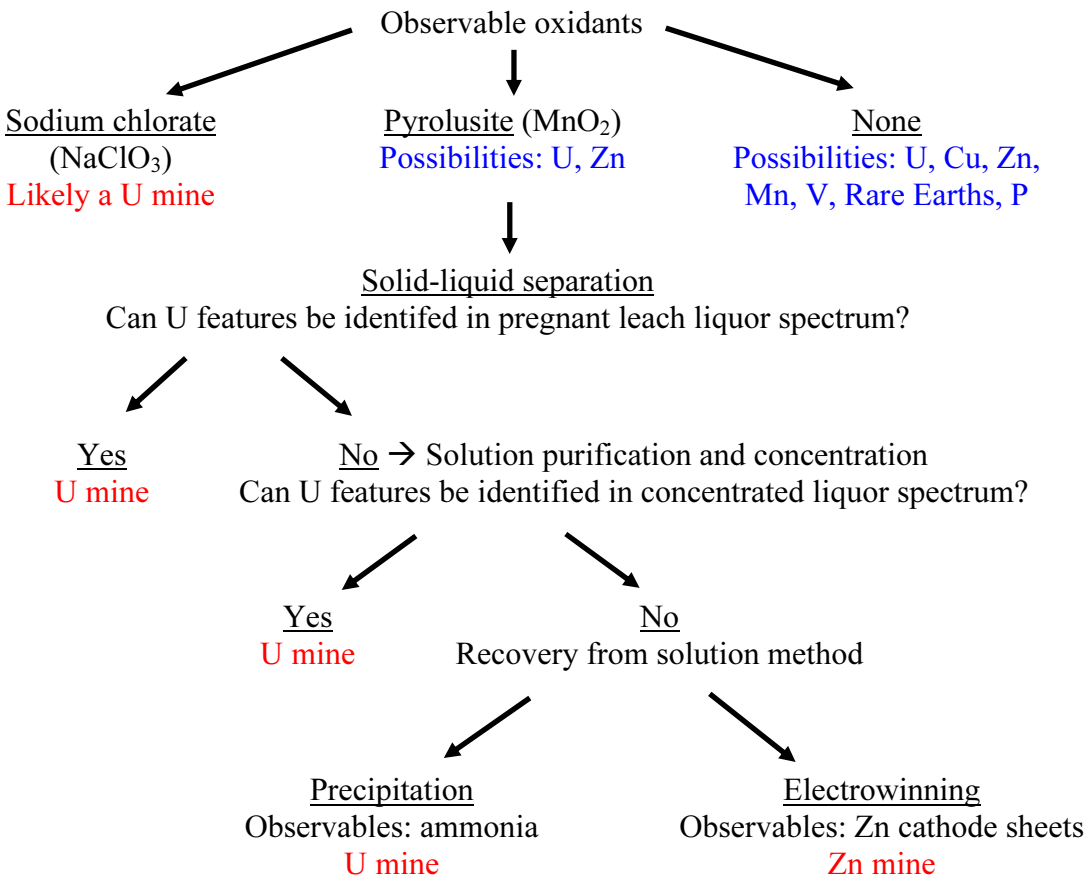

Figure 6(c). Decision tree – sulfuric acid leaching.

This page intentionally left blank.

5. Ranger Site Case Study

In this section, we document promising observables at the Ranger mine and mill. Based on the size, concentration, and spectral characteristics of these promising observables, we then determine whether these promising observables can be identified using current commercial satellite systems, notably Hyperion, ASTER, and Quickbird. Employing the promising observables which can be identified using current commercial satellite systems, we then use the decision tree to make deductions regarding the type of mineral mining and milling activity occurring at the Ranger site.

Table 7 documents the promising observables at the Ranger site. A promising observable is defined as an observable which is exposed (e.g., contained in an uncovered structure), thereby allowing remote spectroscopic identification. Table 7 contains a subset of the potential observables listed in Table 4. For each promising observable, size, concentration, and spectral characteristics are also listed. Utilizing this size, concentration, and spectral information, Table 7 also indicates whether each of the promising observables can be identified using Hyperion, ASTER, and Quickbird. The maximum number of pure pixels each promising observable occupies in a Hyperion, ASTER, and Quickbird satellite image is also listed in Table 7. The pixel number calculations are based on the Hyperion spatial resolution of 30 m, the ASTER spatial resolution of 15 m in the VNIR, and the Quickbird panchromatic spatial resolution of 0.61 m.

Table 7. Promising observables at Ranger mine and mill. For the Hyperion, ASTER, and Quickbird sensors, the table lists the maximum number of pure pixels for each promising observable, and indicates whether the observable can be identified by that sensor (see columns 6-8).

Target	Observables	Size	Concentration	Spectrum	Hyperion	ASTER	Quickbird
Uranium Mining							
Open pit mine	Uraninite (UO_2)	43700 m^2	0-0.5% of volume [7]	[32]	48 pixels / No	194 pixels / No	117441 pixels / No
	Mg chlorite		45% of volume [18]	[33]	48 pixels / Yes	194 pixels / No	117441 pixels / No
	Quartz		37% of volume [18]	[33]	48 pixels / No	194 pixels / No	117441 pixels / No
Discriminator station	Discriminator building	5 m by 8 m	N/A	N/A	0 pixels / No	0 pixels / No	107 pixels / No
Uranium Milling: Leaching							
Sulfur stockpile	Elemental sulfur	9100 m^2	100%	[33]	10 pixels / Yes	40 pixels / No	24455 pixels / No
Uranium Milling: Solid-Liquid Separation							
Thickener	Pregnant leach liquor (UO_2SO_4)	Six 39 m diameter tanks	0.5-1.5 g/L U_3O_8 [23]	[34]	1 pixel per tank / No	4 pixels per tank / No	2889 pixels per tank / No
Clarifying thickener	Pregnant leach liquor (UO_2SO_4)	24 m diameter tank	0.5-1.5 g/L U_3O_8 [23]	[34]	0 pixels / No	2 pixels / No	1215 pixels / No

Table 7 (continued). Promising observables at Ranger mine and mill. For the Hyperion, ASTER, and Quickbird sensors, the table lists the maximum number of pure pixels for each promising observable, and indicates whether the observable can be identified by that sensor (see columns 6-8).

Target	Observables	Size	Concentration	Spectrum	Hyperion	ASTER	Quickbird
Uranium Milling: Solvent Extraction							
Gas leaks from ammonia storage tanks	Ammonia	Unknown, but small	Unknown, but low	[35-38]	No	No	No
Uranium Milling: Tailings Neutralization and Disposal							
Tailings pond (Ranger #1 pit)	Uranium in solution (UO_2^{2+}, UO_2SO_4)	260000 m^2	24 ppm U [27]	[34]	288 pixels / No	1155 pixels / No	698736 pixels / No
	Sulfate ion (SO_4^{2-})		20 g/L SO_4^{2-} [27]	[39-41]	288 pixels / No	1155 pixels / No	698736 pixels / No
Tailings dam	Uranium in solution (UO_2^{2+}, UO_2SO_4)	1 km^2	Unknown, but likely similar to Ranger #1 pit	[34]	1111 pixels / No	4444 pixels / No	2687449 pixels / No
	Sulfate ion (SO_4^{2-})		Unknown, but likely similar to Ranger #1 pit	[39-41]	1111 pixels / No	4444 pixels / No	2687449 pixels / No

Promising observables associated with the Ranger open pit mine include uraninite (UO_2), magnesium chlorite, and quartz. The spectrum for UO_2 [32] is depicted in Figure 7, while Figure 8 depicts the corresponding spectra for magnesium chlorite and quartz in the visible and near infrared [33]. UO_2 cannot be identified using Hyperion, ASTER, or Quickbird due to its very low concentration in the host rock (0-0.5% of volume). In contrast, magnesium chlorite likely can be identified using Hyperion due to the high concentration of this promising observable in the host rock (45% of volume), the large size of the open pit mine (the open pit mine encompasses approximately 48 pixels in a Hyperion image), and the fact that magnesium chlorite has diagnostic spectral features from 2-2.5 μm. In fact, a previous study [42] determined that chlorite could be identified using Hyperion images. Quartz, however, cannot be identified by Hyperion as quartz lacks any distinctive spectral features between 0.4 and 2.5 μm. Magnesium chlorite and quartz cannot be uniquely identified using ASTER or Quickbird due to the limited spectral resolution of these multispectral instruments.

The discriminator station is another promising observable associated with uranium mining at the Ranger site. The discriminator station is small (40 m^2) and does not have a distinguishable spectrum, making it impossible to identify using Hyperion or ASTER. Although the discriminator station does occupy dozens of pixels in a panchromatic Quickbird image, the lack of any distinguishing shape or spectral features prevents its unique identification using Quickbird.

The sulfur stockpile is a promising observable associated with acid leaching at the Ranger site. The spectrum for elemental sulfur is shown in Figure 9 [33]. With an area of 9100 m^2, the sulfur stockpile encompasses approximately 10 pixels in a Hyperion image, 40 pixels in an ASTER image, and 24455 pixels in a panchromatic Quickbird image. The prominent spectral features of elemental sulfur allow its identification using Hyperion. However, unique identification of sulfur would likely not be possible using ASTER and Quickbird due to the limited spectral resolution of these instruments.

Uranyl sulfate (UO_2SO_4) is a promising observable associated with solid-liquid separation. The absorption spectrum of aqueous uranyl sulfate between 340 nm and 500 nm is depicted in Figure 10 [34]. Uranyl sulfate is a weak absorber in the visible with no spectral features between 500 and 700 nm. Aqueous uranyl sulfate shows three strong features in the IR at 1144, 1047, and 956 cm^{-1} [39]. Uranyl sulfate in the thickener or the clarifying thickener cannot be identified using Hyperion due to the instrument's limited spatial resolution (each thickener tank is represented by at most one pure Hyperion pixel, while the clarifying thickener tank is not encompassed by any pure pixels). The fact that aqueous uranyl sulfate is a weak absorber in the visible and does not have any prominent spectral features in the near infrared also limits identification using Hyperion. The relatively low concentration of uranyl sulfate in the thickener and clarifying thickener (0.5-1.5 g/L U_3O_8) also hinders identification using Hyperion. Uranyl sulfate in the thickener and clarifying thickener cannot be identified using ASTER due to the limited spatial resolution of ASTER (each thickener tank is represented by at most 4 pure pixels, and the clarifying thickener tank by at most 2 pixels), the fact that ASTER does not have

any spatial coverage below 500 nm, and the low concentration of this promising observable. Uranyl sulfate in the thickener and clarifying thickener cannot be identified using Quickbird due to the low concentration and the fact that this sensor does not have any spectral coverage in this compound's characteristic absorption regions.

Ammonia is a promising observable used in solvent extraction at the Ranger site. Ammonia exhibits absorption features between 180 and 230 nm [36], but does not have absorption regions in the visible [37]. While ammonia does have characteristic NIR absorption features [38], ammonia's strongest absorption features are observed in the thermal infrared. Figure 11 plots the absorption coefficients for ammonia between 8 and 13 μm [35]. Ammonia that is observable using remote sensing would most likely originate from gas leaks from the ammonia storage tanks. The concentration of ammonia associated with such gas leaks is unknown, but would likely be quite low. The size of such ammonia gas plumes is also an unknown. Ammonia most likely cannot be identified using Hyperion or Quickbird due to the low concentration of ammonia gas in the mill area, and the fact that these sensors have no spectral coverage in the thermal infrared. While ASTER offers limited spectral coverage in the thermal infrared, the low spectral resolution of ASTER would prevent the unique identification of ammonia.

The uranyl ion (UO_2^{2+}) and uranyl sulfate are two promising observables associated with tailings disposal at the Ranger site. The absorption spectra of the aqueous uranyl ion and uranyl sulfate are shown in Figure 10. The uranyl ion and uranyl sulfate are weak absorbers in the visible. The uranyl ion and uranyl sulfate are contained in both the tailings pond (Ranger #1 pit) and the tailings dam. The tailings pond and the tailings dam cover large areas and encompass many pixels in Hyperion, ASTER, and Quickbird images. Despite the large size of these tailings disposal sites, the concentration of uranium in the tailings pond and the tailings dam is very low (24 ppm), preventing identification of the uranyl ion and uranyl sulfate using Hyperion, ASTER, or Quickbird.

The sulfate ion (SO_4^{2-}) is another promising observable contained in the tailings pond and the tailings dam at the Ranger site. The aqueous sulfate ion has a single IR active stretching mode at 1104 cm^{-1} and an IR active bending mode at 613 cm^{-1} [39, 40]. The sulfate ion does not have prominent spectral features in the visible or near infrared regions [41]. Because the sulfate ion lacks distinctive spectral features in spectral regions covered by Hyperion, ASTER, and Quickbird, one could not uniquely identify sulfate ion using these satellite systems.

In summary, based on the size, concentration, and spectral characteristics of the promising observables listed in Table 7, we have determined that magnesium chlorite in the open pit mine and the sulfur stockpile can be identified by Hyperion. Given these identified observables, the decision tree, depicted in Figure 6, is consulted to try to deduce the type of mineral mining and milling activity occurring at the Ranger site. Consulting Figure 6(a), if it was known that magnesium chlorite is a host mineral commonly associated with increased uranium levels in the geographic region encompassed by Ranger, the identification of magnesium chlorite in the open pit mine would be an indicator of uranium mining activity at the Ranger site. Additional evidence, however, would need to be assembled to reach a more definitive conclusion regarding the

type of mineral being mined and milled at Ranger. Next, the section of the decision tree focused on observables associated with leaching, shown in Figure 6(b), is consulted. The identification of the sulfur stockpile at the mill site is an indicator of leaching activity. The type of leaching used at the mill site is acid leaching, as can be ascertained from the presence of sulfur. The fact that sulfuric acid is used at the mill narrows the possible mineral candidates to uranium, copper, zinc, manganese, vanadium, the rare earths, and phosphorus. The lack of additional observables at the mill site prevents any further deductions regarding the type of mining and milling carried out at the site.

It is important to note that while high spatial resolution satellite systems such as Quickbird lack sufficient spectral resolution to uniquely identify many materials, spatial information provided by these systems can complement information obtained from high spectral resolution systems such as Hyperion. As is evident in Figure 5, very few structures in the mill area can be visualized in the Hyperion image. In contrast, the Quickbird image in Figure 4 provides very detailed information on the layout and structures within the mill. One could first locate and measure the mill structures in the Quickbird image. Given the information obtained from the Quickbird image, one could then, if spatial resolution is sufficient, locate these same structures in the Hyperion image and try to identify these structures spectrally. A case in point is the sulfur stockpile, which is clearly distinguishable in the Quickbird image, but encompasses only a few pixels in the Hyperion image.

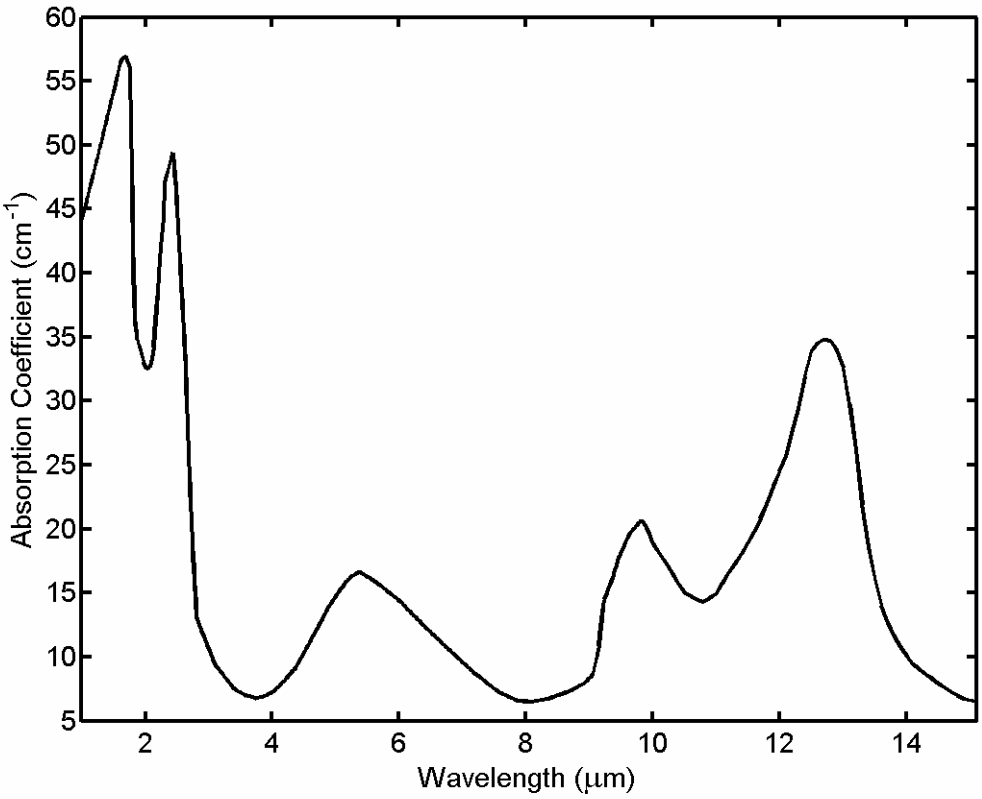

Figure 7. Absorption spectrum for UO_2.

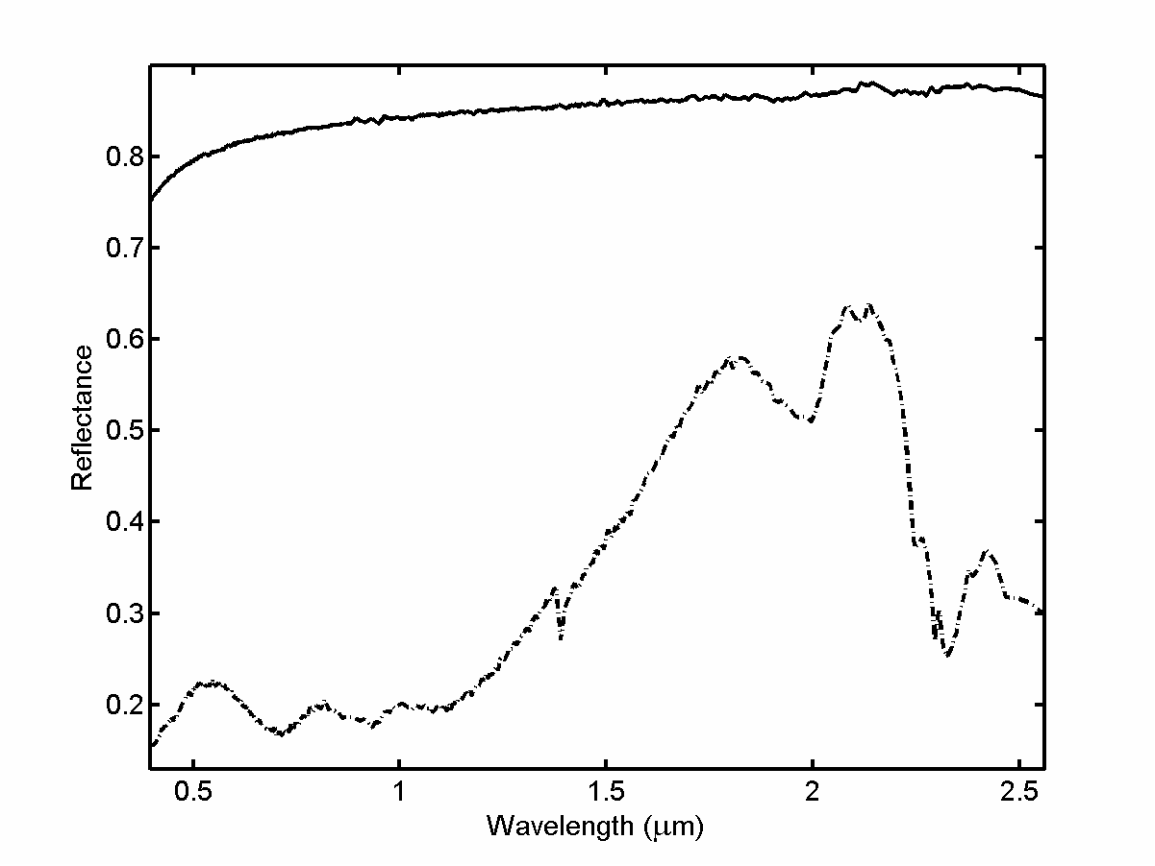

Figure 8. Reflectance spectra for quartz (-) and magnesium chlorite (-.).

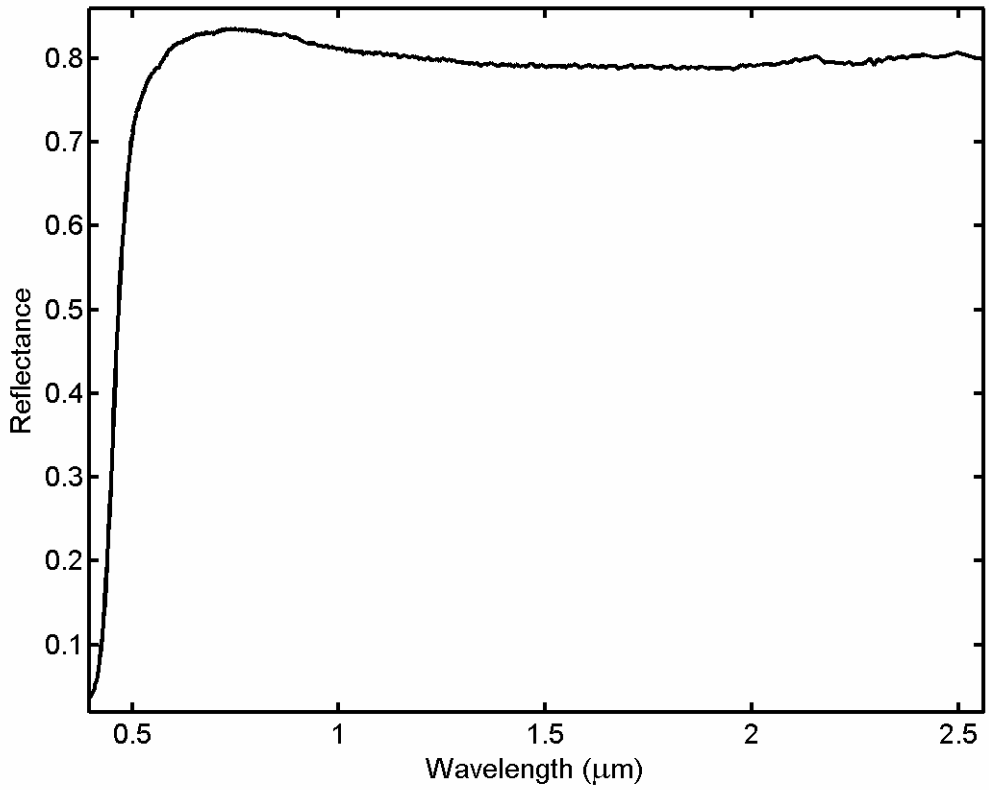

Figure 9. Reflectance spectrum for sulfur.

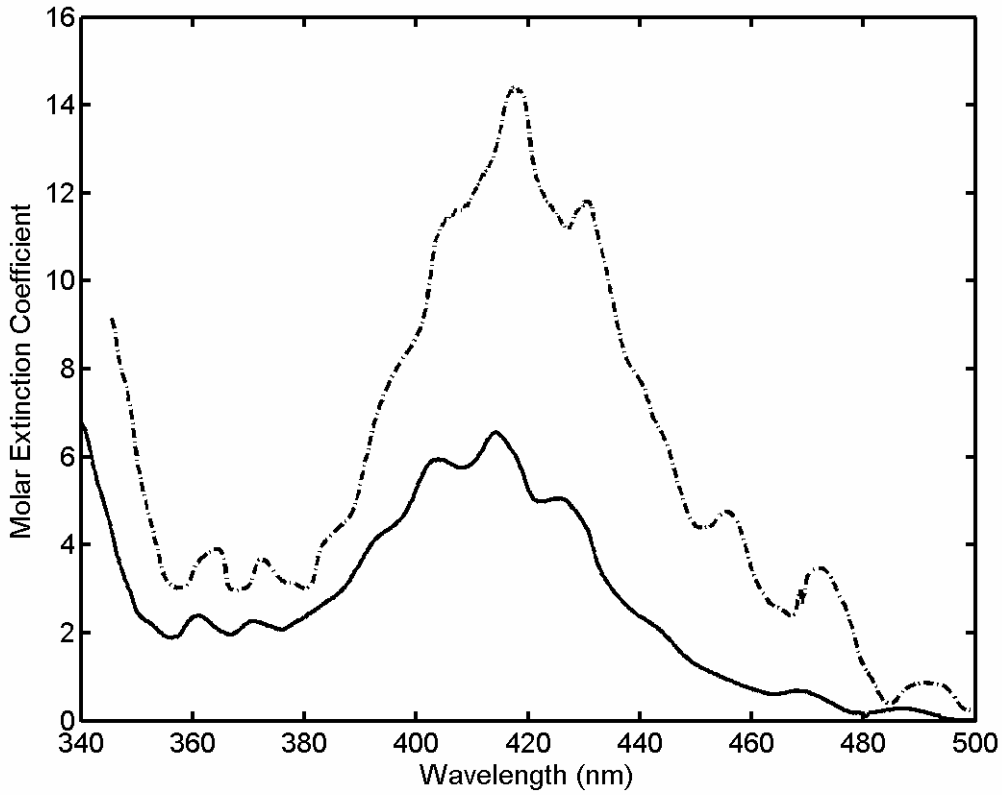

Figure 10. Absorption spectra for aqueous UO_2^{2+} (-) and UO_2SO_4 (-.).

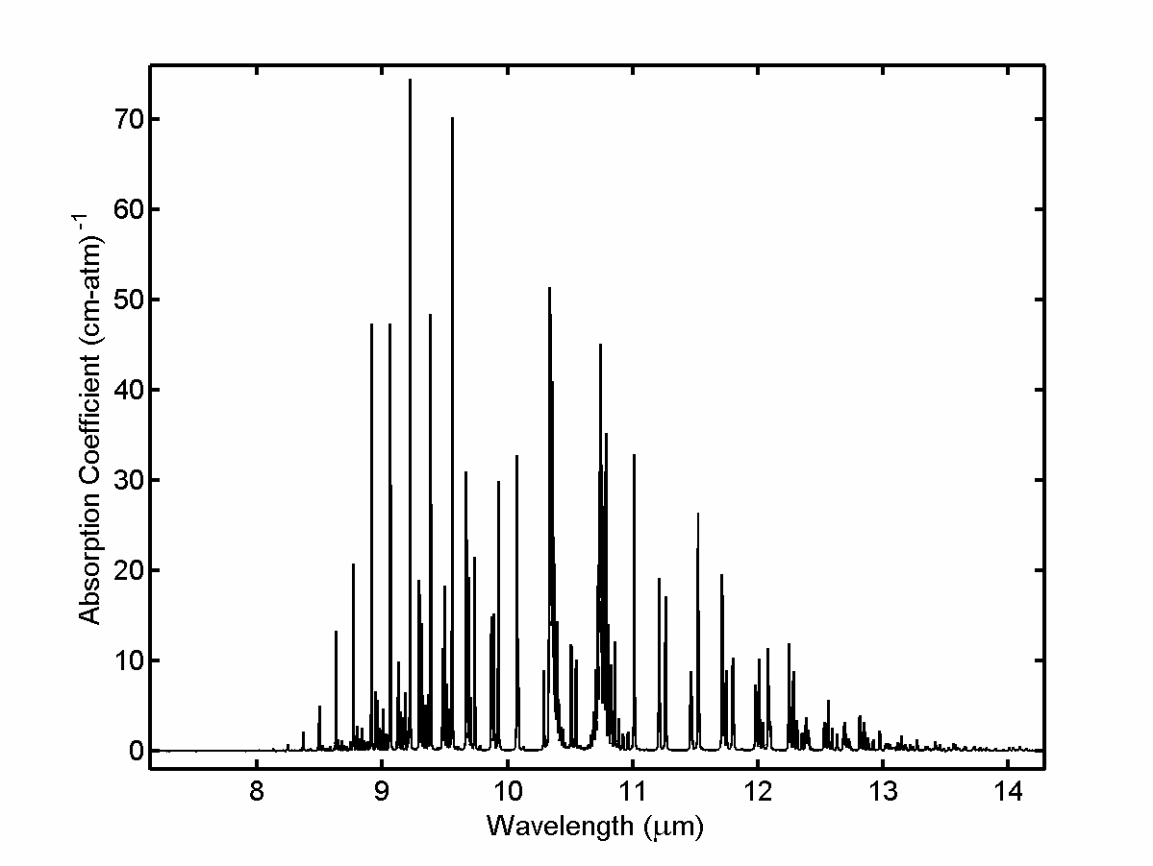

Figure 11. Spectral absorption coefficients for ammonia in the thermal infrared.

This page intentionally left blank.

6. Conclusions

This report documents a systematic evaluation of the ability of current-generation, satellite-based spectroscopic sensors to distinguish uranium mines and mills from other mineral mining and milling operations. We have performed this systematic evaluation by (1) outlining the remote, spectroscopic signal generation process, (2) documenting the capabilities of current commercial satellite systems, (3) systematically comparing the uranium mining and milling process to other mineral mining and milling operations, and (4) identifying the most promising observables associated with uranium mining and milling that can be identified using satellite remote sensing. The Ranger uranium mine and mill in Australia has served as a case study for our systematic analysis. Based on literature research of mineral mining and milling practices, we have developed a decision tree which utilizes the information contained in one or more observables to determine whether uranium is possibly being mined and/or milled at a given site. Promising observables associated with uranium mining and milling at the Ranger site included in the decision tree are uranium ore (typically less than 1 percent uranium by volume), sulfur (used to produce sulfuric acid required in leaching), the uranium pregnant leach liquor (contains uranyl sulfate), ammonia (used in solvent extraction), and uranyl compounds and sulfate ion disposed of in the tailings pond (24 ppm uranium). Based on the size, concentration, and spectral characteristics of these promising observables, we have determined whether these observables can be identified using current commercial satellite systems, namely Hyperion, ASTER, and Quickbird. We conclude that the only promising observables at Ranger that can be uniquely identified using a current commercial satellite system (notably Hyperion) are magnesium chlorite in the open pit mine and the sulfur stockpile. Based on the identified magnesium chlorite and sulfur observables, the decision tree narrows the possible mineral candidates at Ranger to uranium, copper, zinc, manganese, vanadium, the rare earths, and phosphorus, all of which are milled using sulfuric acid leaching.

This page intentionally left blank.

7. References

1. **Uranium 2003: Resources, Production and Demand**: Organization for Economic Cooperation and Development; 2004.
2. Jasani B, Stein G: **Commercial Satellite Imagery: A Tactic in Nuclear Weapon Deterrence**. London: Springer-Verlag; 2002.
3. Truong QS, Borstad GA, Staenz K, Neville RA, Leslie R, Riggs P, Bragin V: **Multispectral and hyperspectral imagery for safeguards and verification of remote uranium mines**.
4. Leslie R, Riggs P, Bragin V, Truong QS, Borstad GA, Neville RA, Staenz K: **Satellite imagery for safeguards purposes: utility of panchromatic and multispectral imagery for verification of remote uranium mines**. In: *Annual Meeting of the Institute of Nuclear Materials Management: June 23-27, 2002; Orlando, FL*; 2002.
5. Neville RA, Staenz K, Levesque J, Nadeau C, Truong QS, Borstad GA: **Uranium mine detection using an airborne imaging spectrometer**. In: *Fifth International Airborne Remote Sensing Conference: September 17-20, 2001; San Francisco, CA*; 2001.
6. Levesque J, Neville RA, Staenz K, Truong QS: **Preliminary results on the investigation of hyperspectral remote sensing for the identification of uranium mine tailings**. In: *Proceedings of the ISSSR: June 10-15, 2001; Quebec City, Canada*; 2001.
7. **Ranger Uranium Mine**. *Mining Magazine* 1985, **153**(5):392-403.
8. Schowengerdt RA: **Remote Sensing: Models and Methods for Image Processing**. San Diego, CA: Academic Press; 1997.
9. Dahlkamp FJ: **Uranium Ore Deposits**. Berlin: Springer-Verlag; 1993.
10. Hardy CJ: **The chemistry of uranium milling**. *Radiochimica Acta* 1978, **25**(3-4):121-134.
11. **Extraction and beneficiation of ores and minerals, volume 5, uranium**. In. Washington, D.C.: U.S. Environmental Protection Agency, Office of Solid Waste, Special Waste Branch; 1995.
12. Dahlkamp FJ: **Classification of uranium deposits**. *Miner Deposita* 1978, **13**(1):83-104.
13. Peterson EC: **Uranium**. In: *SME Mineral Processing Handbook.* Edited by Weiss NL. New York, NY: Society of Mining Engineers of the American Institute of Mining, Metallurgical, and Petroleum Engineers; 1985: 24-21 - 24-41.
14. Wills BA: **Mineral Processing Technology**. Oxford, England: Butterworth-Heinemann; 1997.
15. Woody RJ, George DR: **Acid leaching of uranium ores**. In: *Uranium Ore Processing.* Edited by Clegg JW, Foley DD. Reading, MA: Addison-Wesley Publishing Company; 1958: 115-152.
16. McClaine LA: **Carbonate leaching of uranium ores**. In: *Uranium Ore Processing.* Edited by Clegg JW, Foley DD. Reading, MA: Addison-Wesley Publishing Company; 1958: 153-171.

17. Kendall CJ: **Ranger uranium deposits**. In: *Geology of the Mineral Deposits of Australia and Papua New Guinea.* Edited by Hughes FE. Melbourne: The Australasian Institute of Mining and Metallurgy; 1990: 799-805.
18. Savory PJ: **Geology and grade control at ERA - Ranger Mine, Northern Territory, Australia**. In: *1994 AusIMM Annual Conference on Australian Mining Looks North - The Challenges and Choices; Darwin, Australia*: Australasian Inst Mining & Metallurgy; 1994: 97-101.
19. Johnston A, Needham S: **Protection of the environment near the Ranger uranium mine**. In: *Supervising Scientist.* Canberra, Australia: Environment Australia; 1999: 38.
20. Jones D, Topp H, Russell H, Davidson J, Levy V, Gilderdale M, David G, Ring R, Conway G, Macintosh P *et al*: **Process water treatment at the Ranger uranium mine, Northern Australia**. *Water Science and Technology* 2003, **47**(10):155-162.
21. Milner EF: **Lead and zinc concentrates: extraction processes and schedules**. In: *SME Mineral Processing Handbook.* Edited by Weiss NL. New York, NY: Society of Mining Engineers of the American Institute of Mining, Metallurgical, and Petroleum Engineers; 1985: 15-10.
22. Dahlstrom DA, Emmett RCJ: **Solid-liquid separations**. In: *SME Mineral Processing Handbook.* Edited by Weiss NL. New York, NY: Society of Mining Engineers of the American Institute of Mining, Metallurgical, and Petroleum Engineers; 1985: 13-26 - 13-33.
23. Kennedy RH: **The winning of uranium**. In: *SME Mineral Processing Handbook.* Edited by Weiss NL. New York, NY: Society of Mining Engineers of the American Institute of Mining, Metallurgical, and Petroleum Engineers; 1985: 24-31 - 24-32.
24. Gupta CK, Mukherjee TK: **Hydrometallurgy in Extraction Processes,** vol. II. Boca Raton, FL: CRC Press; 1990.
25. Gupta CK, Mukherjee TK: **Hydrometallurgy in Extraction Processes,** vol. I. Boca Raton, FL: CRC Press; 1990.
26. Sheng Y, Peter P, Milnes AR: **Instrumentation and monitoring behaviour of uranium tailings deposited in a deep pit**. In: *7th International Conference on Tailings and Mine Waste 00: January 23-26, 2000; Fort Collins, CO*: AA Balkema; 2000: 91-100.
27. **Investigation of the potable water contamination incident at Ranger mine March 2004**. In. Darwin, NT: Australian Government, Department of the Environment and Heritage; 2004: 56, 125, 200-201, 285, 291.
28. **Extraction and beneficiation of ores and minerals, volume 4, copper**. In. Washington, D.C.: U.S. Environmental Protection Agency, Office of Solid Waste, Special Waste Branch; 1994.
29. Holmes JA, Deuchar AD, Stewart LN, Parker JD: **Design, construction and commissioning of the Nchanga tailings leach plant**. In: *Extractive Metallurgy of Copper, Volume II, Hydrometallurgy and Electrowinning.* Edited by Yannopoulos JC, Agarwal JC, vol. II. Baltimore, MD: Port City Press; 1976: 907-925.

30. Fletcher AW, Finkelstein NP, Derry R: **Leaching systems**. In: *SME Mineral Processing Handbook.* Edited by Weiss NL. New York, NY: Society of Mining Engineers of the American Institute of Mining, Metallurgical, and Petroleum Engineers; 1985: 13-17 - 13-23.
31. Ross AH, Mackiw VN: **Hydrometallurgy**. In: *SME Mineral Processing Handbook.* Edited by Weiss NL. New York, NY: Society of Mining Engineers of the American Institute of Mining, Metallurgical, and Petroleum Engineers; 1985: 13-11 - 13-79.
32. Bates JL: **Visible and infrared absorption spectra of uranium dioxide**. *Nuclear Science and Engineering* 1965, **21**(1):26-29.
33. Clark RN, Swayze GA, Gallagher AJ, King TVV, Calvin WM: **The U.S. Geological Survey, Digital Spectral Library: Version 1: 0.2 to 3.0 microns**. U.S. Geological Survey; 1993.
34. Rabinowitch E, Belford RL: **Spectroscopy and Photochemistry of Uranyl Compounds**. New York, NY: The MacMillan Company; 1964.
35. Sharpe SW, Johnson TJ, Sams RL, Chu PM, Rhoderick GC, Johnson PA: **Gas-phase databases for quantitative infrared spectroscopy**. *Applied Spectroscopy* 2004, **58**(12):1452-1461.
36. Mellqvist J, Rosen A: **DOAS for flue gas monitoring. I. Temperature effects in the UV/visible absorption spectra of NO, NO_2, SO_2 and NH_3.** *Journal of Quantitative Spectroscopy and Radiative Transfer* 1996, **56**(2):187-208.
37. Mellqvist J, Axelsson H, Rosen A: **DOAS for flue gas monitoring. III. In-situ monitoring of sulfur dioxide, nitrogen monoxide and ammonia.** *Journal of Quantitative Spectroscopy and Radiative Transfer* 1996, **56**(2):225-240.
38. Lundsberg-Nielsen L, Hegelund F, Nicolaisen FM: **Analysis of the high-resolution spectrum of ammonia ($^{14}NH_3$) in the near-infrared region, 6400-6900 cm^{-1}.** *Journal of Molecular Spectroscopy* 1993, **162**(1):230-245.
39. Gal M, Goggin PL, Mink J: **Vibrational spectroscopic studies of uranyl complexes in aqueous and non-aqueous solutions.** *Spectrochimica Acta, Part A (Molecular Spectroscopy)* 1992, **48A**(1):121-132.
40. Ross SD: **Sulphates and other oxy-anions of Group VI**. In: *The Infrared Spectra of Minerals.* Edited by Farmer VC. London: Mineralogical Society of London; 1974: 423-444.
41. Lund Myhre CE, Christensen DH, Nicolaisen FM, Nielsen CJ: **Spectroscopic study of aqueous H_2SO_4 at different temperatures and compositions: variations in dissociation and optical properties.** *Journal of Physical Chemistry A* 2003, **107**(12):1979-1991.
42. Cudahy TJ, Hewson R, Huntington JF, Quigley MA, Barry PS: **The performance of the satellite-borne Hyperion hyperspectral VNIR-SWIR imaging system for mineral mapping at Mount Fitton, South Australia.** In: *IEEE 2001 International Geoscience and Remote Sensing Symposium Proceedings, July 9-13, 2001, Sydney, Australia;* 2001, vol. 311: 314-316.

Distribution:

1	MS0123	Donna L. Chavez	01011
1	MS0406	Jody L. Smith	05712
1	MS0886	Christopher L. Stork	01823
1	MS0887	Duane B. Dimos	01800
1	MS0888	Doug Wall	01823
1	MS1361	Heidi A. Smartt	06923
1	MS1371	Dianna S. Blair	06926
2	MS9018	Central Technical Files	8945-1
2	MS0899	Technical Library	9616


Sandia National Laboratories